JGR Atmospheres

RESEARCH ARTICLE
10.1029/2023JD040436

Impact of Atmospheric Compressibility and Stokes Drift on the Vertical Transport of Heat and Constituents by Gravity Waves

Chester S. Gardner[1]

[1]Department of Electrical and Computer Engineering, University of Illinois, Urbana, IL, USA

Key Points:

- Non-breaking gravity waves induce strong vertical transport that depends on compressibility of wave fluctuations and wave-driven Stokes drift
- Theory compares favorably with observations of the mesopause region at midlatitudes
- Results can be used to parameterize transport of heat & constituents induced by unresolved waves in global chemistry-climate models

Supporting Information:

Supporting Information may be found in the online version of this article.

Correspondence to:

C. S. Gardner,
cgardner@illinois.edu

Citation:

Gardner, C. S. (2024). Impact of atmospheric compressibility and stokes drift on the vertical transport of heat and constituents by gravity waves. *Journal of Geophysical Research: Atmospheres*, *129*, e2023JD040436. https://doi.org/10.1029/2023JD040436

Received 20 NOV 2023
Accepted 24 MAR 2024
Corrected 18 MAY 2024

This article was corrected on 18 MAY 2024. See the end of the full text for details.

Author Contribution:

Conceptualization: Chester S. Gardner
Data curation: Chester S. Gardner
Formal analysis: Chester S. Gardner
Funding acquisition: Chester S. Gardner
Methodology: Chester S. Gardner
Project administration: Chester S. Gardner
Software: Chester S. Gardner
Validation: Chester S. Gardner
Visualization: Chester S. Gardner
Writing – original draft: Chester S. Gardner

Abstract Vertical transport of heat and atmospheric constituents by gravity waves plays a crucial role in shaping the thermal and constituent structure of the middle atmosphere. We show that atmospheric mixing by non-breaking waves can be described as a diffusion process where the potential temperature (K_H) and constituent (K_{Wave}) diffusivities depend on the compressibility of the wave fluctuations and the vertical Stokes drift imparted to the atmosphere by the wave spectrum. K_H and K_{Wave} are typically much larger than the eddy diffusivity (K_{zz}), arising from the turbulence generated by breaking waves, and can exceed several hundred m^2s^{-1} in regions of strong wave dissipation. We also show that the total diffusion of heat and constituents caused by waves, turbulence, and the thermal motion of molecules, is enhanced in the presence of non-breaking waves by a factor that is proportional to the variance of the wave-driven lapse rate fluctuations. Diffusion enhancements of both heat and constituents of 50% or more can be experienced in regions of low atmospheric stability, where the lapse rate fluctuations are large. These important transport effects are not currently included in most global chemistry-climate models, which typically only consider the eddy diffusion that is induced when the unresolved, but parameterized waves, experience dissipation. We show that the theoretical results compare favorably with observations of the mesopause region at midlatitudes and describe how the theory may be used to more fully account for the unresolved wave transport in global models.

Plain Language Summary Winds blowing over topography and weather systems in the lower atmosphere can generate waves that propagate into the upper atmosphere to the edge of space, where their amplitudes become very large in response to decreasing atmospheric density. These waves drive the global circulation of the middle and upper atmosphere and can even affect satellite orbits and space weather. They also play very important roles in transporting heat and constituents vertically by mixing the atmosphere, which causes diffusion, and by inducing a net vertical motion, called Stokes drift. Unfortunately, global chemistry-climate models cannot resolve the important small-scale waves, which make the largest contributions to wave transport. Existing models account for wave transport by simply calculating the eddy mixing by turbulence that arises when waves break. We develop a general theory to describe wave-driven diffusion and advection of heat and constituents in the atmosphere and show how the theory can be used to estimate the transport caused by unresolved, non-breaking waves in atmospheric models. These results are important because they demonstrate the significance of wave transport, apart from simple eddy mixing, and provide a method for incorporating this crucial, but currently missing process, in future global chemistry-climate models.

1. Introduction

Gravity waves, generated by orography and storm systems in the lower atmosphere, propagate upwards and are a ubiquitous feature of the mesosphere and lower thermosphere (MLT). Vertical transport of heat and constituents by gravity waves is an important process that has a significant impact on the thermal and constituent structure of the atmosphere, especially at higher altitudes where wave amplitudes are large (Gardner & Liu, 2007, 2010; Guo & Liu, 2021; Hickey et al., 2000; Liu & Gardner, 2004; Walterscheid, 1981; Walterscheid & Schubert, 1989; Weinstock, 1983; Xu et al., 2003). Local wave effects contribute to vertical transport via five mechanisms. Non-breaking waves mix the atmosphere thereby contributing to diffusive transport. Dissipating and breaking waves also contribute to diffusive transport by generating turbulence. Furthermore, diffusion is enhanced in the presence of waves because the wave fluctuations amplify the vertical gradients of potential temperature and constituent mixing ratios. The vertical Stokes drift, induced by waves (e.g., Coy et al., 1986; Walterscheid & Hocking, 1991), results in advective transport of heat and constituents. And lastly, waves drive the chemical transport of reactive

species by modulating their chemical reactions (Gardner & Liu, 2016; Walterscheid & Schubert, 1989). Wave-driven residual circulation in the MLT, which results in both horizontal and vertical transport, is another important global process, but is not addressed in the current paper.

In the MLT gravity wave periods (τ) range from the buoyancy period ($\tau_B \sim 5$ min) to the inertial period ($\tau_i \sim 12$ hr and longer), vertical wavelengths (λ_z) range from ~1 km to 100–200 km, and horizontal wavelengths (λ_h) range from a few km up to global scale. Because most global chemistry-climate models cannot fully resolve the important smaller-scale waves ($\tau < \sim 2$ hr, $\lambda_z < \sim 10$ km, $\lambda_h < \sim 1{,}000$ km), wave transport associated with these unresolved waves is typically parameterized by simply calculating the eddy diffusion generated when the parameterized waves experience dissipation or completely break (e.g., Beres et al., 2004). Observations of the mesopause region have shown that this overly simplified approach is inadequate, at least when modeling the mesospheric metal layers (Carrillo-Sanchez et al., 2016; Feng et al., 2013; Gardner & Liu, 2007, 2010; Gardner et al., 2017; Huang et al., 2015; Marsh et al., 2013; Plane et al., 2015).

Researchers have attempted to account for enhanced wave transport in global models by deriving scaling factors that effectively amplify the down gradient eddy mixing of constituents (Grygalashvyly et al., 2012; Nakamura, 2001; Winters & D'Asaro, 1996). However, this approach does not account for atmospheric mixing by non-breaking waves, which is characterized by effective constituent (K_{Wave}) and thermal (potential temperature, K_H) diffusivities. Both diffusivities can be expressed in terms of the sensible heat and wave energy fluxes. Although the heat flux cannot be derived from existing wave parameterization schemes, Gardner et al. (2019) showed how K_{Wave} and K_H can be estimated in terms of the eddy diffusivity and the variances of the wave-driven temperature and lapse rate fluctuations. Liu (2021) employed a global model and the concept of scale invariance to infer the thermal diffusivity of the unresolved, small-scale waves from the modeled K_H values of the resolved, large-scale waves. Most recently, Guarino et al. (2024) implemented the K_{Wave}/K_H parameterization proposed by Gardner et al. (2019) in the Whole Atmosphere Community Climate Model (WACCM, e.g. Gettelman et al., 2019) and explored the impact on modeled upper atmosphere CO_2, Na, Fe, and temperature. Mesospheric CO_2 and temperature were significantly impacted by including the additional wave mixing, while the enhanced wave-induced vertical transport largely reconciled the modeled Na and Fe layers with their estimated meteoric injection rates.

In this paper, we focus on wave-induced transport of heat and chemically inert constituents. We generalize the solutions for K_{Wave} and K_H originally derived by Gardner et al. (2019), to expand the range of applicability for both parameters and to include the impact of atmospheric compressibility and Stokes drift. We show how the vertical gradients of potential temperature and species mixing ratios are on average larger in the presence of waves so that transport by molecular diffusion, eddy mixing, and wave mixing are all enhanced. We derive solutions for the vertical flux of potential temperature, first, by assuming that weak dissipation introduces phase shifts into the gravity wave polarization relations, and second, by solving the advection-diffusion equation for heat transport. These solutions are then used to derive new expressions for K_{Wave} and K_H that are compared with lidar observations of the mesopause region. Finally, we discuss how these new results can be used to parameterize the wave transport of heat and constituents by non-breaking, unresolved waves in modern global chemistry-climate models.

2. Wave-Induced Vertical Constituent Flux

We consider the constituent density and potential temperature fluctuations and the resultant vertical fluxes induced by a spectrum of non-breaking gravity waves. The vertical fluxes are defined as the expected values of the products of the vertical wind fluctuations (w') with the species density (ρ'_C) and potential temperature (θ') fluctuations. To simplify the calculations, we assume that the species is chemically inert, and initially, only consider the vertical fluxes that are imparted by wave-induced mixing and advection. Later, we generalize the results to include the important effects of molecular diffusion and of turbulence caused by breaking waves.

Fick's First Law of Diffusion states that the diffusive flux is directed from regions of high concentration to regions of lower concentration, where the flux magnitude is proportional to the concentration gradient and the proportionality constant is the diffusion coefficient. This relationship was originally deduced from observations in liquids but has subsequently been shown to characterize diffusive transport in solids, liquids, and gases, including molecular diffusion in the atmosphere caused by Brownian motion and eddy mixing caused by the random motions of atmospheric turbulence. To motivate the following theoretical calculations and to provide physical

insight, we first explore the characteristics of the constituent fluxes induced by non-breaking gravity waves, by assuming that the constituent transport associated with wave fluctuations can also be modeled as Fickian diffusion. Gravity wave motions are highly anisotropic (e.g., Eckermann & Vincent, 1989) so that the wave-induced mixing and concomitant diffusion are also expected to be anisotropic. Here we focus on the vertical diffusion of inert constituents which is caused by the vertical atmospheric displacements associated with the gravity wave vertical wind fluctuations. By applying Fick's First Law to the vertical flux of the constituent mixing ratio, we obtain.

$$\overline{w'\left(\frac{\rho_C}{\rho_A}\right)'} = -K_{Wave}\frac{\partial}{\partial z}\overline{\left(\frac{\rho_C}{\rho_A}\right)} \simeq -K_{Wave}\frac{\partial}{\partial z}\left(\frac{\overline{\rho}_C}{\overline{\rho}_A}\right) \tag{1}$$

The symbols ρ_C and ρ_A are, respectively, the constituent and atmospheric densities, w is the vertical wind velocity, and K_{Wave} is the effective vertical diffusivity caused by waves. The overbar denotes the mean quantities (ensemble average), and the prime denotes the wave-induced perturbations. By linearizing the left-hand-side of Equation 1 and solving for the constituent flux, we obtain.

$$\overline{w'\rho_C'} \simeq \overline{\rho}_C\frac{\overline{w'\rho_A'}}{\overline{\rho}_A} - \overline{\rho}_C K_{Wave}\frac{1}{\left(\overline{\rho}_C/\overline{\rho}_A\right)}\frac{\partial\left(\overline{\rho}_C/\overline{\rho}_A\right)}{\partial z} \tag{2}$$

The term

$$\frac{\overline{w'\rho_A'}}{\overline{\rho}_A} \simeq -\left(\frac{\overline{w'T'}}{\overline{T}} - \frac{\overline{w'p'}}{\overline{p}}\right) \tag{3}$$

is the normalized atmospheric mass flux which is closely related to the vertical Stokes drift velocity imparted to the atmosphere by the gravity waves, where T is temperature and p is pressure. Stokes drift is usually defined as the difference between the average Lagrangian and Eulerian vertical velocities (Andrews & McIntyre, 1978). Coy et al. (1986) showed that for gravity waves, the vertical Stokes drift is equal to the normalized mass flux given by Equation 3. Thus, if constituent transport by waves is modeled as a Fickian diffusion process, then the vertical constituent flux given by Equation 2 is composed of two terms; (a) the advective flux associated with Stokes drift and (b) the diffusive flux associated with atmospheric mixing, which is characterized by the diffusion coefficient K_{Wave}. For chemically active species there is a third term (not considered here), viz. the chemical flux associated with wave perturbations of the species chemistry (Gardner & Liu, 2016).

In the following we make no assumptions about the form of the wave transport process and directly compute the vertical constituent flux $\left(\overline{w'\rho_C'}\right)$ after first solving the continuity equation for the wave induced species perturbations $\left(\rho_C'\right)$. The constituent density fluctuations are governed by the advection-diffusion equation (i.e., continuity equation), which for chemically inert neutral species is given by (e.g., Grygalashvyly et al., 2012; Smith et al., 2011).

$$\frac{\partial\rho_c}{\partial t} + \nabla\cdot\left(\underline{V}\rho_C\right) = \nabla\cdot\left[K_{Wave}\rho_A\nabla\left(\rho_C/\rho_A\right)\right] \simeq \frac{\partial}{\partial z}\left[K_{Wave}\rho_A\frac{\partial\left(\rho_C/\rho_A\right)}{\partial z}\right] \tag{4}$$

$\underline{V} = \overline{V} + \underline{V}'$ is the velocity vector where $\overline{V}$ is the mean background wind vector and $\underline{V}'$ represents the gravity wave perturbations. To generalize the flux calculations, we seek solutions for the species fluctuations that are independent of the unperturbed species profile. To do so, we need to transform the continuity Equation 4 into another set of three differential equations that are largely independent of ρ_C. This can be accomplished by employing an appropriate model for the spatial variations of ρ_C. We make the reasonable assumption that the unperturbed species and atmospheric densities are horizontally homogeneous. In this case the perturbed densities may be expressed in the form

$$\rho_C(x, y, z, t) = e^{-\delta_C-\chi}\rho_{C0}(z-\zeta) \tag{5}$$

$$\rho_A(x, y, z, t) = e^{-\chi}\rho_{A0}(z-\zeta) \simeq \rho_{A0}\exp[-\chi-(z-\zeta)/H_A]. \tag{6}$$

$H_A = \frac{\overline{T}}{(g/R + \partial\overline{T}/\partial z)}$ is the atmospheric density scale height, $g = 9.5\ \mathrm{ms}^{-2}$ is the gravitational acceleration (@ $z = 100$ km), and $R = 287\ \mathrm{m^2K^{-1}s^{-2}}$ is the gas constant for dry air. By substituting Equation 5 into Equation 4 we find that the wave parameters ζ, χ, and δ_C are solutions to the following partial differential equations.

$$\frac{\partial \zeta}{\partial t} = w' - \underline{V}' \cdot \nabla \zeta \tag{7}$$

$$\frac{\partial \chi}{\partial t} = \nabla \cdot \underline{V}' - \underline{V}' \cdot \nabla \chi \tag{8}$$

$$\frac{\partial \delta_C}{\partial t} = -\frac{1}{\rho_C}\frac{\partial}{\partial z}\left[K_{Wave}\rho_A \frac{\partial(\rho_C/\rho_A)}{\partial z}\right] - \underline{V}' \cdot \nabla \delta_C \tag{9}$$

Under this transformation, if ζ, χ, and δ_C are solutions to Equations 7–9, respectively, then ρ_C given by Equation 5 is a solution to the continuity equation given by Equation 4. Furthermore, ζ and χ, which depend on the wind fluctuations, are independent of the species profile, as desired. This is not surprising since wave propagation and the resulting wind fluctuations, are not affected by the minor species composition of the atmosphere. On the other hand, diffusion effects, which are embodied in δ_C, are dependent on the species profile. The generalization for horizontally inhomogeneous species is presented in Gardner and Shelton (1985) and addressed in Appendix C. The generalization for chemically active species is described in Gardner and Liu (2016) and Gardner (2018). For our purposes here, those features may be neglected but can easily be added later, if desired. According to Equations 7–9, ζ is related to the vertical displacements caused by the vertical wind fluctuations of the waves, χ is related to the compressibility of the wave fluctuations $\left(\nabla \cdot \underline{V}'\right)$, and δ_C is related to the effective diffusivity acting on ρ_C.

The constituent flux can now be computed by multiplying ρ_C (Equation 5) by w' and averaging the result. If we assume that ζ, χ, and δ_C are small and retain only the first-order terms of the perturbation series expansion of ρ_C, then the constituent flux can be expressed in terms of the vertical fluxes of ζ, χ, and δ_C and the unperturbed constituent profile ρ_{C0}. However, the small perturbation constraint can be relaxed by noting that ζ, χ, and δ_C are the combined effects of numerous nonbreaking waves, generated by many different (independent) sources. According to the Central Limit Theorem, all three parameters are approximately, jointly distributed Gaussian random processes. Consequently, the constituent and atmospheric density fluxes can be expressed in closed form (see Equations 9–12 in Gardner & Liu, 2010)

$$\overline{w'\rho_C{}'} = \overline{w' e^{-\delta_C - \chi}\rho_{C0}(z-\zeta)} = -\overline{\rho}_C \overline{w'\delta_C} - \overline{\rho}_C \overline{w'\chi} - \frac{\partial \overline{\rho}_C}{\partial z}\overline{w'\zeta}, \tag{10}$$

$$\overline{w'\rho_A{}'} = \overline{w' e^{-\chi}\rho_{A0}(z-\zeta)} = -\overline{\rho}_A \overline{w'\chi} - \frac{\partial \overline{\rho}_A}{\partial z}\overline{w'\zeta}, \tag{11}$$

and from Appendix A

$$\overline{w'\delta_C} \simeq K_{Wave}\frac{\xi_{inst}}{(\overline{\rho}_C/\overline{\rho}_A)}\frac{\partial(\overline{\rho}_C/\overline{\rho}_A)}{\partial z}, \tag{12}$$

where

$$\xi_{inst} = \frac{\mathrm{Var}\left(\partial T'/\partial z\right)}{\left(\Gamma_{ad} + \partial\overline{T}/\partial z\right)^2}. \tag{13}$$

$\Gamma_{ad} = g/C_p = 9.5 \times 10^{-3}\ \mathrm{Km}^{-1}$ is the adiabatic lapse rate and $C_p = 1{,}003\ \mathrm{m^2K^{-1}s^{-2}}$ is the specific heat at constant pressure. The instability parameter ξ_{inst} is approximately equal to the mean of the inverse Richardson number and is a measure of the instability of the atmosphere through which the waves are propagating. In the mesopause region, ξ_{inst} generally varies between about 0.1 and 0.5, but can exceed 0.5 in regions of strong perturbations and

dissipation (e.g., Fig. 3f in Chu et al., 2022). By combining Equations 10–12 we obtain for the total constituent flux, in the absence of turbulence and molecular diffusion,

$$\overline{w'\rho_C{}'} \simeq \overline{\rho}_C \frac{\overline{w'\rho_A{}'}}{\overline{\rho}_A} - \overline{\rho}_C \overline{w'\zeta'} \frac{(1+\xi_{inst})}{(\overline{\rho}_C/\overline{\rho}_A)} \frac{\partial(\overline{\rho}_C/\overline{\rho}_A)}{\partial z}. \quad (14)$$

Equation 14 is nearly identical to (2), the constituent flux derived from Fick's First Law, with $K_{Wave} = \overline{w'\zeta}$. The only difference is the enhancement of the diffusive flux by the factor ($1+\xi_{inst}$), which arises because, in the presence of wave fluctuations, the mean vertical mixing ratio gradient of the constituent is enhanced. Grygalashvyly et al. (2012) employed a different mathematical approach to show that molecular and turbulent diffusion are also enhanced in the presence of waves by a factor which they call the mixing efficiency. By applying the wave polarization relations, it is not difficult to show that their enhanced diffusivity, which they denote K_{Waves} (Equation 14, Grygalashvyly et al., 2012), is characterized by an enhancement factor that is nearly identical to ξ_{inst}.

To summarize, Equation 14 was derived by ignoring chemistry, assuming the unperturbed constituent density profile ρ_{C0} depended only on z, and assuming the perturbed constituent and atmospheric densities could be expressed as the right-hand-sides of Equations 5 and 6 where the wave parameters ζ, χ, and δ_C are Gaussian processes. All the assumptions up to this point are reasonable. Furthermore, Equation 14 is nearly equivalent to Fick's First Law of Diffusion applied to the constituent mixing ratio, viz. Equation 2. We now derive expressions for K_{Wave} and K_H.

3. Effective Wave-Induced Constituent (K_{Wave}) and Thermal (K_H) Diffusivities

Gardner and Shelton (1985) derived solutions to Equations 7 and 8 for a single gravity wave that obeys the polarization and dispersion relations under the constraint that its vertical wavelength (λ_z) satisfies the inequality $\lambda_z << 4\pi H_A$. They did this by expanding ζ and χ in a perturbation series, assuming that the velocity perturbations were caused by a traveling wave, and then applying the gravity wave polarization and dispersion relations. Here we derive a more general solution that weakens the constraint on λ_z and highlights the impact of atmospheric compressibility. First, we note that ζ and χ are independent of the constituent profile (see Equations 7 and 8). Consequently, the solutions for ζ and χ apply for any non-dissipating or weakly dissipating gravity wave that satisfies the linearized equation for mass conservation (i.e., linearized continuity equation for atmospheric density, Equation 11 in Vadas, 2013). Solving the mass conservation equation for $\nabla \cdot \underline{V}'$ associated with a single monochromatic gravity wave, in a coordinate system that is moving with the unperturbed wind field, we find.

$$\nabla \cdot \underline{V}' = -\frac{1}{\overline{\rho}_A}\left(\frac{\partial \rho'_A}{\partial t} + \underline{V}' \cdot \nabla \overline{\rho}_A\right) = -i\omega \frac{\rho'_A}{\overline{\rho}_A} + \frac{w'}{H_A} \quad (15)$$

By applying the gravity wave polarization relation that relates ρ'_A and w' for fully compressible, non-dissipating waves (Equation B10 in Vadas, 2013), we obtain

$$\frac{\rho'_A}{\overline{\rho}_A} = -\frac{iN^2}{\omega g} \frac{\left[1 - \frac{i}{\gamma m H_A}\left(\frac{\gamma}{2} - \frac{\omega^2}{N^2}\right)\right]}{\left[1 - \frac{i}{\gamma m H_A}\left(\frac{\gamma}{2} - 1\right)\right]} w' = -\frac{iN^2}{\omega g} \frac{\left[1 + \frac{1}{(\gamma m H_A)^2}\left(\frac{\gamma}{2} - \frac{\omega^2}{N^2}\right)^2\right]^{1/2}}{\left[1 + \frac{1}{(\gamma m H_A)^2}\left(\frac{\gamma}{2} - 1\right)^2\right]^{1/2}} e^{i\varphi_\rho} w', \quad (16)$$

where

$$\varphi_\rho = -\tan^{-1}\left[\frac{1}{\gamma m H_A}\left(\frac{\gamma}{2} - \frac{\omega^2}{N^2}\right)\right] + \tan^{-1}\left[\frac{1}{\gamma m H_A}\left(\frac{\gamma}{2} - 1\right)\right]. \quad (17)$$

N is the buoyancy frequency, ω is the wave frequency, $m = 2\pi/\lambda_z$ is the vertical wavenumber, λ_z is the vertical wavelength, and $\gamma = 1.4$ is the ratio of specific heats. Substituting Equation 16 into Equation 15 and taking the real part yields

$$\nabla \cdot \underline{V}' = \frac{\psi}{H_A} w', \tag{18}$$

where

$$\psi = 1 - \frac{N^2}{g} H_A \frac{\left[1 + \frac{1}{(\gamma m H_A)^2}\left(\frac{\gamma}{2} - \frac{\omega^2}{N^2}\right)^2\right]^{\frac{1}{2}}}{\left[1 + \frac{1}{(\gamma m H_A)^2}\left(\frac{\gamma}{2} - 1\right)^2\right]^{\frac{1}{2}}} \cos \varphi_\rho \simeq 1 - \tilde{\kappa} \text{ for } \lambda_z \ll \frac{2^{3/2}\pi\gamma H_A}{\sqrt{\gamma - 1}} \simeq 120 \text{ km} \tag{19}$$

and

$$\tilde{\kappa} = \frac{N^2}{g} H_A = \frac{\left(\Gamma_{ad} + \partial \overline{T}/\partial z\right)}{\left(g/R + \partial \overline{T}/\partial z\right)}. \tag{20}$$

After substituting the right-hand-side of Equation 18 into Equation 8, we see that $\chi = \frac{\psi}{H_A}\zeta$. If we now use the exponential model for the atmospheric density given by Equation 6, the final solutions for ζ and χ for a single wave are.

$$\zeta = \frac{H_A}{(1-\psi)} \ln\left(\frac{\rho_A}{\overline{\rho}_A}\right) = \frac{g}{N^2} \ln\left(\frac{\rho_A}{\overline{\rho}_A}\right) \tag{21}$$

$$\chi = \frac{\psi}{(1-\psi)} \ln\left(\frac{\rho_A}{\overline{\rho}_A}\right) = \left(\frac{g}{N^2 H_A} - 1\right) \ln\left(\frac{\rho_A}{\overline{\rho}_A}\right) \tag{22}$$

Now let's consider what happens when the wind fluctuations are caused by a spectrum of gravity waves. For λ_z<<120 km, ψ/H_A given by Equation 19 is a constant that is identical for each wave. Because Equation 18 is a linear equation, while Equations 7 and 8 are not, if each wave in the spectrum obeys the linearized equation for mass conservation given by Equations 15 and 18, then these equations also hold for the spectrum of waves because $\underline{V}'$, ρ'_A and w′ are the sums of the contributions from all the waves. Therefore, (21) and (22) are also solutions to (7) and (8) for the spectrum of waves. In this case, because ρ'_A and w′ are both Gaussian distributed, K_{Wave} is

$$K_{Wave} = \frac{g}{N^2} \overline{w' \ln\left(1 + \frac{\rho_A'}{\overline{\rho}_A}\right)} = \frac{\frac{g}{N^2}\frac{\overline{w'\rho_A'}}{\overline{\rho}_A}}{\left[1 - \frac{\mathrm{Var}\left(\rho_A'\right)}{\overline{\rho}_A^{\,2}}\right]} \tag{23}$$

Equation 23 was obtained without placing any constraint on the wave amplitudes. The right-hand-side of Equation 23 was derived by expanding the logarithm in a power series and using the identity for the expectation of the product of multiple, mutually distributed, zero-mean Gaussian random variables. When $\frac{\mathrm{Var}\left(\rho_A'\right)}{\overline{\rho}_A^{\,2}} \sim \frac{\mathrm{Var}\left(T'\right)}{\overline{T}^2} \ll 1$, which is easily satisfied throughout the stratosphere, mesosphere, and lower thermosphere, then Equation 23 simplifies to $K_{Wave} \simeq \frac{g}{N^2}\frac{\overline{w'\rho_A'}}{\overline{\rho}_A}$.

No physical mechanisms were invoked to derive the solution for the constituent flux given by Equation 14 and the effective wave diffusivity given by Equation 23. However, K_{Wave} is proportional to the vertical Stokes drift velocity, which suggests that wave-driven diffusion may arise from mixing of the atmosphere by the cumulative actions of the Stokes velocities contributed by each wave in the spectrum. Walterscheid and Hocking (1991) called this mixing process Stokes diffusion and used an entirely different mathematical approach to analyze its characteristics. They showed that a spectrum of gravity waves induces a Lagrangian drift of atmospheric parcels that varies spatially and consequently, the atmospheric parcels drift apart in a manner analogous to diffusion. By evaluating parcel motions under the influence of a spectrum of waves, they showed that the associated diffusion

coefficients were on the order of 10^2 m^2s^{-1}. Unfortunately, their expression for the "Stokes" diffusion coefficient, which they defined in analogy with molecular diffusion and expressed in terms of the mean square vertical separation between atmospheric parcels and the period over which the separation was calculated (Equation 29, Walterscheid & Hocking, 1991), cannot be readily compared to K_{Wave}.

Weinstock (1976, 1990) also considered atmospheric mixing that arises from non-linear interactions among all the waves in the spectrum. Although he was primarily concerned with the viscous damping of the wave amplitudes caused by the mixing process, not diffusion of constituents and heat, Weinstock (1990, Equation 12c) did derive an expression for the effective wave diffusivity by retaining appropriate nonlinear terms in the wave equation. As will be shown later, his expression for diffusion is similar, but not identical, to K_{Wave}. The exact solution for K_{Wave} given by Equation 23 was derived without placing any constraints on wave amplitudes, so the effects of the nonlinear wave-wave interactions analyzed by Weinstock (1990), as well as Stokes diffusion analyzed by Walterscheid and Hocking (1991), should both be included in the analysis and solution described here.

Turbulence and molecular diffusion also make important contributions to the vertical constituent flux. The total vertical flux of constituent C, denoted by F_C^z, is obtained by recomputing $\overline{w'\delta_C}$ and $\overline{w'\rho_C{}'}$ by replacing K_{Wave} with the total atmospheric diffusivity $\left(K_{Wave} + K_{zz} + K_C^m\right)$ in Equation 12 (see Appendix A) and by adding the fluxes associated with turbulence and molecular diffusion to Equation 14.

$$F_C^z \simeq \overline{\rho}_C \frac{\overline{w'\rho'_A}}{\overline{\rho}_A} - \overline{\rho}_C\left(K_{Wave} + K_{zz} + K_C^m\right)\frac{\left(1+\xi_{inst}\right)}{\left(\overline{\rho}_C/\overline{\rho}_A\right)}\frac{\partial\left(\overline{\rho}_C/\overline{\rho}_A\right)}{\partial z} \tag{24}$$

K_{zz} is the eddy diffusivity for turbulence and K_C^m is the molecular diffusivity for species C.

We are also interested in the wave-induced thermal diffusivity (K_H), which is related to the vertical flux of potential temperature (θ). Potential temperature is defined as $\theta = T\left(p_0/p\right)^{R/C_p}$, where p_0 is the reference pressure. Like the constituent flux given by Equation 24, the total vertical flux of potential temperature (F_θ^z) is composed of two terms, the advective thermal flux induced by the vertical Stokes drift imparted to the atmosphere by the spectrum of waves and the total diffusive flux caused by wave mixing, turbulence, and molecular diffusion (see derivation in Appendix B).

$$F_\theta^z \simeq \overline{\theta}\frac{\overline{w'\rho'_A}}{\overline{\rho}_A} - \overline{\theta}\left(K_H + K_{zz} + K_H^m\right)\frac{\left(1+\xi_{inst}\right)}{\overline{\theta}}\frac{\partial\overline{\theta}}{\partial z}. \tag{25}$$

K_H and K_{zz} are, respectively, the effective thermal diffusivities for waves and for turbulence, and K_H^m is the molecular diffusivity for heat, which is given by

$$K_H^m = \mu\,\mathrm{Pr}\frac{T^{2/3}}{\rho_A}, \tag{26}$$

where $\mu \simeq 3.55 \times 10^{-7}$ $kgs^{-1}m^{-1}$ $K^{-2/3}$ is an experimental parameter and Pr is the Prandtl number (see Section 6.6.2.1 https://ncar.github.io/CAM/doc/build/html/cam5_scientific_guide/extensions.html#gravity-wave-drag). Because pressure fluctuations induced by turbulence are negligible, the eddy diffusivities for heat and constituents are both equal to K_{zz}.

The factor $(1+\xi_{inst})$ in Equations 24 and 25 accounts for the enhancement of the mean vertical gradients of the species mixing ratio and potential temperature by the wave-induced fluctuations in p, T, ρ_C, and ρ_A. ξ_{inst} varies with altitude and for the Starfire Optical Range (SOR) annual mean data set (Gardner & Liu, 2007, 2010), the enhancement of the diffusion components of the vertical fluxes ranges from about 20% to 50% (see Table S1 in Supporting Information). At McMurdo, by employing a much shorter 40 hr data set spanning 78–112 km, Chu et al. (2022, Figure 3f) reported that ξ_{inst} ranged from about 30% to about 60%. Thus, the enhancement of constituent and heat diffusion can be significant, at least in the mesopause region.

It is convenient to also define a parameter (K_E) associated with the gravity wave energy flux $\left(\overline{w'p'}\right)$, which can be written in terms of the temperature and lapse rate variances by expressing the wave-driven p' spectrum in terms of the T' spectrum using the gravity wave polarization relations (Liu, 2009; see Appendix A, Chu et al., 2022).

$$K_E = \frac{g}{N^2}\frac{R}{C_p}\frac{\overline{w'p'}}{\overline{p}} \simeq \beta(s,q)\left(1-2\alpha_{down}\right)\frac{\Gamma_{ad}}{\overline{T}}\sqrt{\frac{Var\left(T'\right)}{Var\left(\partial T'/\partial z\right)}}\frac{fVar\left(T'\right)}{\left(\Gamma_{ad}+\partial\overline{T}/\partial z\right)^2} \tag{27}$$

$\Gamma_{ad} = g/C_p$ is the adiabatic lapse rate, α_{down} is the fraction of wave energy that is propagating downward, f is the inertial frequency, and β is a dimensionless parameter that depends on the distribution of wave energy versus vertical wavenumber and temporal frequency (see Equation(A-7), Chu et al., 2022). By combining Equations 23 and 27 with the definition of θ' and linearizing the equations, we also obtain.

$$K_{Wave} = -\frac{g}{N^2}\left(\frac{\overline{w'T'}}{\overline{T}} - \frac{\overline{w'p'}}{\overline{p}}\right) = \left(\frac{C_p}{R}-1\right)K_E - \frac{g}{N^2}\frac{\overline{w'\theta'}}{\overline{\theta}} \tag{28}$$

$$K_H = K_{Wave} - \frac{g}{N^2}\frac{\overline{w'\theta'}}{\overline{\theta}} = \left(\frac{C_p}{R}-1\right)K_E - 2\frac{g}{N^2}\frac{\overline{w'\theta'}}{\overline{\theta}} \tag{29}$$

$$\frac{g}{N^2}\frac{\overline{w'T'}}{\overline{T}} = K_E + \frac{g}{N^2}\frac{\overline{w'\theta'}}{\overline{\theta}} \tag{30}$$

$$\frac{g}{N^2}\frac{\overline{w'\theta'}}{\overline{\theta}} = \frac{g}{N^2}\left(\frac{\overline{w'T'}}{\overline{T}} - \frac{R}{C_p}\frac{\overline{w'p'}}{\overline{p}}\right) \tag{31}$$

These wave mixing parameters are summarized in Table 1. The key to calculating K_{Wave} and K_H is calculating the wave-driven potential temperature flux $\overline{w'\theta'}$, which is generally (but not always) zero for non-dissipating waves and is generally (but not always) negative for dissipating waves. Both K_{Wave} and K_H are mostly positive, and they become much larger when the wave spectrum is dominated by upwardly propagating waves that are experiencing some dissipation (i.e., when $\overline{w'\theta'} < 0$). In the absence of dissipation $\overline{w'\theta'} = 0$ so that both K_{Wave} and K_H are equal to $\left(\frac{C_p}{R}-1\right)K_E$. K_H is not zero for non-dissipating waves because downward diffusion of heat is required to balance the upward advective transport of heat caused by Stokes drift. In contrast, the sensible heat flux is positive in regions dominated by upwardly propagating waves experiencing no dissipation, but $\overline{w'T'}$ eventually becomes negative as dissipation increases. As mentioned earlier, Weinstock (1990) derived an expression for the effective wave diffusivity caused by nonlinear wave-wave interactions, which he denoted D. If one modifies Weinstock's expression for D to include the impact of downward propagating wave energy, its not difficult to show that in the absence of dissipation $K_{Wave} = K_H \simeq 2(1-R/C_P)D$. In Section 4 we compute $\overline{w'\theta'}$ by assuming that weak dissipation induces small phase shifts in the gravity wave polarization relations. In Section 5 we compute $\overline{w'\theta'}$ by solving the linearized advection-diffusion equation for heat transfer.

4. Calculating the Potential Temperature Flux by Modifying the Phases of the Wave Polarization Relations

To incorporate wave-mixing into global chemistry-climate models to account for the transport induced by the unresolved, non-breaking, parameterized waves, it is necessary to express K_{Wave}, K_H, and K_E in terms of parameters such as K_{zz}, $Var(T')$ and $Var(-\partial T'/\partial z)$, that can be derived from the models' gravity wave parameterization schemes. Recently, Gardner et al. (2019) linearized the advection-diffusion equation for heat transfer to derive solutions for K_{Wave} and K_H by assuming the wave-induced fluctuations are incompressible $\left(\nabla\cdot\underline{V}' = 0\right)$. Although incompressibility has been widely applied in studies of gravity wave fluctuations (e.g., Fritts & Dunkerton, 1985; Liu, 2000), the assumption is clearly incompatible with the form of the linearized equations for mass conservation, viz. Equations 15 and 18, that were used to derive the solutions for ζ, χ, and K_{Wave} given by

Table 1
Summary of Key Wave Mixing Parameters for the Real Atmosphere w/Stokes Drift

Parameter	Formula[a,b]	Eq. #
Total Vertical Constituent Flux for Chemically Inert Species	$F_C^z \simeq \overline{\rho}_C \frac{\overline{w'\rho'_A}}{\overline{\rho}_A} - \overline{\rho}_C \left(K_{Wave} + K_{zz} + K_C^m\right) \frac{\left(1+\xi_{inst}\right)}{\left(\overline{\rho}_C/\overline{\rho}_A\right)} \frac{\partial\left(\overline{\rho}_C/\overline{\rho}_A\right)}{\partial z}$	(24)
Total Vertical Flux of Potential Temperature	$F_\theta^z \simeq \overline{\theta} \frac{\overline{w'\rho'_A}}{\overline{\rho}_A} - \overline{\theta}\left(K_H + K_{zz} + K_H^m\right) \frac{\left(1+\xi_{inst}\right)}{\overline{\theta}} \frac{\partial\overline{\theta}}{\partial z}$	(25)
Wave-Induced Vertical Stokes Drift Velocity	$\frac{\overline{w'\rho'_A}}{\overline{\rho}_A} = -\left(\frac{\overline{w'T'}}{\overline{T}} - \frac{\overline{w'p'}}{\overline{p}}\right) = \frac{N^2}{g} K_{Wave}$	(23)
Equivalent Diffusivity for Wave Energy Flux	$K_E = \frac{g}{N^2}\frac{R}{C_p}\frac{\overline{w'p'}}{\overline{p}} \simeq \beta(s,q)\left(1-2\alpha_{down}\right)\frac{\Gamma_{ad}}{\overline{T}}\sqrt{\frac{Var\left(T'\right)}{Var\left(\partial T'/\partial z\right)}}\ \frac{fVar\left(T'\right)}{\left(\Gamma_{ad}+\partial\overline{T}/\partial z\right)^2}$	(32)
Wave-Induced Constituent Diffusivity	$K_{Wave} = -\frac{g}{N^2}\left(\frac{\overline{w'T'}}{\overline{T}} - \frac{\overline{w'p'}}{\overline{p}}\right) = \left(\frac{C_p}{R}-1\right)K_E - \frac{g}{N^2}\frac{\overline{w'\theta'}}{\overline{\theta}}$	(28)
Wave-Induced Thermal Diffusivity	$K_H = K_{Wave} - \frac{g}{N^2}\frac{\overline{w'\theta'}}{\overline{\theta}} = \left(\frac{C_p}{R}-1\right)K_E - 2\frac{g}{N^2}\frac{\overline{w'\theta'}}{\overline{\theta}}$	(29)
Wave-Induced Vertical Flux of Sensible Heat	$\frac{g}{N^2}\frac{\overline{w'T'}}{\overline{T}} = K_E + \frac{g}{N^2}\frac{\overline{w'\theta'}}{\overline{\theta}}$	(30)
Wave-Induced Vertical Flux of Potential Temperature	$\frac{g}{N^2}\frac{\overline{w'\theta'}}{\overline{\theta}} = \frac{g}{N^2}\left(\frac{\overline{w'T'}}{\overline{T}} - \frac{R}{C_p}\frac{\overline{w'p'}}{\overline{p}}\right)$	(32) (36)
	$= \begin{cases} -\varepsilon(q)\exp\left[-Var\left(\Delta\phi_{w'T'}\right)/2\right]\sin\left(\overline{\Delta\phi_{w'T'}}\right)\dfrac{fVar\left(T'\right)}{\left(\Gamma_{ad}+\partial\overline{T}/\partial z\right)^2} \\ \dfrac{-\tilde{\kappa}\xi_{inst}}{\left(\overline{\psi}+\tilde{\kappa}-2\tilde{\kappa}\xi_{inst}\right)}\left[\left(\dfrac{C_p}{R}-1\right)K_E + K_{zz} + K_H^m\right] \end{cases}$	

[a]$\beta(s,q)$ and $\varepsilon(q)$ are defined, respectively, by Equations A7 and 15 in Chu et al. (2022). [b]ξ_{inst} is defined by Equation 13, ψ by Equation 18, and $\tilde{\kappa}$ by Equation 20 in this paper.

Equations 21–23. Here we take a different approach by calculating K_{Wave}, K_H, and K_E directly from the polarization relations for weakly dissipating gravity waves.

Although several researchers have derived the gravity wave polarization relations beginning with Hines (1960), we employ the polarization relations derived by Vadas (2013) for fully compressible, non-dissipating waves. Chu et al. (2022) considered the additional phase shifts between w' and p' $\left(\Delta\phi_{w'p'}\right)$ and w' and T' $\left(\Delta\phi_{w'T'}\right)$ that are caused by weak dissipation. Because w' and p' are approximately 180° out of phase, small phase shifts make negligible contributions to the energy flux and K_E. Therefore, $\Delta\phi_{w'p'}$ does not appear in Equation 27. In contrast, w' and T' are approximately 90° out of phase, so the additional phase shift associated with weak dissipation makes a significant contribution to the potential temperature flux (see Equations 14–16, Chu et al., 2022)

$$\frac{g}{N^2}\frac{\overline{w'\theta'}}{\overline{\theta}} \simeq -\varepsilon(q)\exp\left[-\frac{Var\left(\Delta\phi_{w'T'}\right)}{2}\right]\sin\left(\overline{\Delta\phi_{w'T'}}\right)\frac{fVar\left(T'\right)}{\left(\Gamma_{ad}+\frac{\partial\overline{T}}{\partial z}\right)^2}, \tag{32}$$

where $\varepsilon(q)$ is given by Equation 15 in Chu et al. (2022). Notice that for non-dissipating waves where $\Delta\phi_{w'T'} = 0$, the potential temperature flux is zero and so the scaled sensible heat flux, given by Equations 30, is equal to K_E, which is positive if most of the wave energy is propagating upward.

Lu et al. (2017) measured the phase differences between w' and T' for 184 mesoscale waves observed between 85 and 100 km at Table Mt., CO. They found that the mean phase difference (84.2°) was $\overline{\Delta\phi_{w'T'}} = 2.6°$ larger than the phase difference predicted by the polarization relations (81.6°), and the standard deviation was 26.7°. They suggested that the excess phase shift was likely caused by dissipation associated with damping by eddy and molecular viscosity. Damping of wave amplitudes by the viscosity of the atmosphere was first examined by Hines (1960) and later extended by Pitteway and Hines (1963) to include both viscous and conductive dissipation. The theory was further extended by Weinstock (1976, 1990) to include wave-induced damping. Superimposed on

the coherent motions of an atmospheric wave are the random thermal motions of individual molecules (molecular viscosity), and the larger-scale random motions imparted by turbulence and the full spectrum of waves. The mixing associated with these multi-scale processes degrades the organized bulk motion imparted to the atmosphere by an individual wave, leading to attenuation of the wave, and a positive shift of the phase between w' and T' as observed by Lu et al. (2017).

5. Calculating the Potential Temperature Flux by Solving the Advection-Diffusion Equation for Heat Transfer

Potential temperature is a conserved quantity for an air parcel in adiabatic motion, that is, for wave motions in which there are no heat sources and sinks. We assume this condition applies in the MLT, so that the potential temperature fluctuations, induced by gravity waves and turbulence, are described by the advection-diffusion equation for heat transfer (e.g., see Equation 3, Fritts & Dunkerton, 1985).

$$\frac{\partial \theta}{\partial t} + \nabla \cdot (\underline{V}\theta) = \nabla \cdot \left[\left(K_H + K_{zz} + K_H^m \right) \nabla \theta \right] \tag{33}$$

K_H^m, the molecular diffusivity for heat given by Equation 26, increases with increasing altitude and only becomes significant in the thermosphere where the atmospheric density is small, and the temperature is large. Versions of Equation 33 have also been called the thermodynamic equation by Walterscheid (1981), the thermodynamic energy equation by Fritts and Dunkerton (1985), and the thermal equation by Liu (2000). The sum $\left(K_H + K_{zz} + K_H^m\right)$ represents the total background thermal diffusivity (viscosity) of the atmosphere arising from mixing by waves, turbulence, and the thermal motion of atmospheric molecules. By assuming that both the mean flow and the wave perturbations are incompressible ($\nabla \cdot \underline{V} = 0$), several authors have analyzed linearized versions of Equation 33 (Equation 1 in Walterscheid, 1981; Equation 7 in Fritts & Dunkerton, 1985; Equation 1 in Liu, 2000; Equation 16 in Gardner et al., 2019).

As shown by Vadas (2013) and others, non-dissipating waves that obey the mass conservation equation are fully compressible ($\psi = 1 - \tilde{\kappa}$). Atmospheric turbulence generated by dissipating waves is usually assumed to be incompressible ($\psi = 0$) because the resulting density fluctuations are small. We proceed with a more general analysis by assuming that for wave perturbations, the atmospheric density fluctuations partially satisfy the linearized equation for mass conservation so that the divergence of the wind fluctuations is given by Equations 15 and 18, where the compressibility parameter ψ may be different for each wave in the spectrum. We also ignore wind shear and assume that the unperturbed wind velocity is zero, which is equivalent to solving (33) in a coordinate system that is moving with the mean wind. In this case the linearized version of Equation 33 is

$$\frac{\partial \theta'}{\partial t} + \overline{\theta} \nabla \cdot \underline{V}' + \underline{V}' \cdot \nabla \overline{\theta} = \left(K_H + K_{zz} + K_H^m \right) \nabla^2 \theta' + \nabla \left(K_H + K_{zz} + K_H^m \right) \cdot \nabla \theta'. \tag{34}$$

To proceed, we multiply both sides of Equation 34 by θ', noting that $\overline{\theta}$ depends only on altitude (z), and then compute the mean.

$$\overline{\theta} \sum_i \left(\frac{\psi_i}{H_A} \overline{w_i' \theta_i'} \right) + \frac{\partial \overline{\theta}}{\partial z} \sum_i \left(\overline{w_i' \theta_i'} \right) \simeq (\overline{\psi}/\tilde{\kappa} + 1) \frac{N^2 \overline{\theta}}{g} \overline{w' \theta'} \simeq - \left(K_H + K_{zz} + K_H^m \right) \overline{\nabla \theta' \cdot \nabla \theta'} \tag{35}$$

The subscripts on the perturbed quantities denote the contribution from the ith wave in the spectrum. In deriving (35) we applied the mean value theorem to the first summation, where $\overline{\psi}$ represents the effective mean compressibility of the spectrum of wave fluctuations, which varies with altitude. We also assumed that $K_H + K_{zz} + K_H^m$ varies slowly with position, while θ' and $\nabla\theta'$ are approximately in phase quadrature, so that the term involving $\nabla\left(K_H + K_{zz} + K_H^m\right)$ in Equation 34 can be neglected.

By substituting the expression for K_H given by Equations 29 into 35 and solving for the potential temperature flux, we obtain

Table 2
Starfire Optical Range, NM Annual Mean Data[a]

Z (km)	$-\frac{g}{N^2}\frac{\overline{w'\theta'}}{\overline{\theta}}$ (m^2/s)	$-\frac{g}{N^2}\frac{\overline{w'T'}}{\overline{T}}$ (m^2/s)	K_{zz} Gaussian model (m^2/s)	K_E $\alpha_{down} = 0.15$ (m^2/s)	K_H (m^2/s)	K_{Wave} (m^2/s)	$\overline{\Delta\phi_{wT'}}$ (deg)	$\overline{\psi}$	$\frac{\overline{\psi}}{1-\tilde{\kappa}}$ (%)
100	39.6	10.8	1.7	28.8	151	111	5.6	0.117	16.4
99	44.0	10.4	3.0	33.6	172	128	6.7	0.012	1.6
98	24.2	−5.9	5.1	30.1	123	99.3	4.3	0.018	2.4
97	11.1	−13.3	8.4	24.4	83.1	72.0	2.2	0.208	28.1
96	9.2	−12.4	13.4	21.6	72.3	63.1	1.8	0.429	57.5
95	14.5	−7.5	20.4	22.0	83.9	69.4	2.5	0.426	57.0
94	33.0	9.5	29.6	23.2	124	90.9	5.3	0.274	36.8
93	60.3	38.5	41.8	21.8	175	115	9.8	0.187	25.5
92	91.6	70.6	56.2	21.0	236	144	15.1	0.155	21.4
91	134	112	73.2	21.6	322	188	21.8	0.134	18.6
90	172	152	91.0	20.2	394	222	30.7	0.120	16.8
89	183	166	109	16.6	405	223	41.3	0.019	2.7
88	177	162	125	14.8	391	214	47.9	−0.028	−4.1
87	167	151	138	16.1	374	207	43.2	−0.038	−5.5
86	159	140	147	19.1	366	207	35.5	−0.020	−2.8
85	160	139	150	21.2	373	213	30.6	0.044	5.9
Mean							**19°**	**0.129**	**17.4%**

[a]Table S1, Supporting Information, This paper.

$$\frac{g}{N^2}\frac{\overline{w'\theta'}}{\overline{\theta}} \simeq \frac{-\tilde{\kappa}\xi_{inst}}{\left(\overline{\psi}+\tilde{\kappa}-2\tilde{\kappa}\xi_{inst}\right)}\left[\left(\frac{C_p}{R}-1\right)K_E + K_{zz} + K_H^m\right], \quad (36)$$

where ξ_{inst} is given by Equation 13. The key wave mixing parameters are summarized in Table 1 in terms of the mean compressibility parameter $\overline{\psi}$ for the wave spectrum and the total atmospheric diffusivity (viscosity) contributed by non-dissipating waves $\left(\left(\frac{C_p}{R}-1\right)K_E\right)$, turbulence ($K_{zz}$) and the thermal motion of atmospheric molecules $\left(K_H^m\right)$.

6. Comparison With Observations

To assess the efficacy of the wave mixing parameters given in Table 1, we employ the extensive lidar measurements of wind, temperature, and the vertical fluxes of sensible heat and Na made in the mesopause region at the Starfire Optical Range (SOR, 34.96°N, 106.46°W) on the Kirtland Air Force Base near Albuquerque, NM (Gardner & Liu, 2007, 2010). The annual mean values of the fundamental parameter profiles employed in our calculations are summarized in Table S1 of the Supporting Information. K_E, K_{Wave}, and K_H were computed using the SOR data set and the profiles are tabulated in Table 2. Obviously, transport by non-breaking waves in the mesopause region is significant as K_{Wave} and K_H can each exceed several hundred m^2s^{-1}. Next, we derive profiles of the mean phase shift and compressibility from this data set to confirm that the values are realistic.

K_E is calculated using Equation 27 for $s = 1$ and $q = 2$, which are the values commonly observed at mid-latitudes. Although gravity waves are primarily generated in the lower atmosphere by orographic forcing, convection, and frontogenesis associated with storm systems, in the MLT downward propagating waves can arise from upper-level reflections, ducting, and the generation of downward propagating secondary waves, when primary waves break. The fraction of wave energy propagating downward in the MLT varies over a wide range and can even exceed 50% in regions of strong wave breaking (Chu et al., 2022; Vadas & Becker, 2018; Vadas et al., 2018). Although α_{down} can depend on altitude, for simplicity, here we assume $\alpha_{down} = 0.15$, which is the value derived from a hodograph analysis of monochromatic waves observed at SOR between 85 and 100 km (Hu et al., 2002).

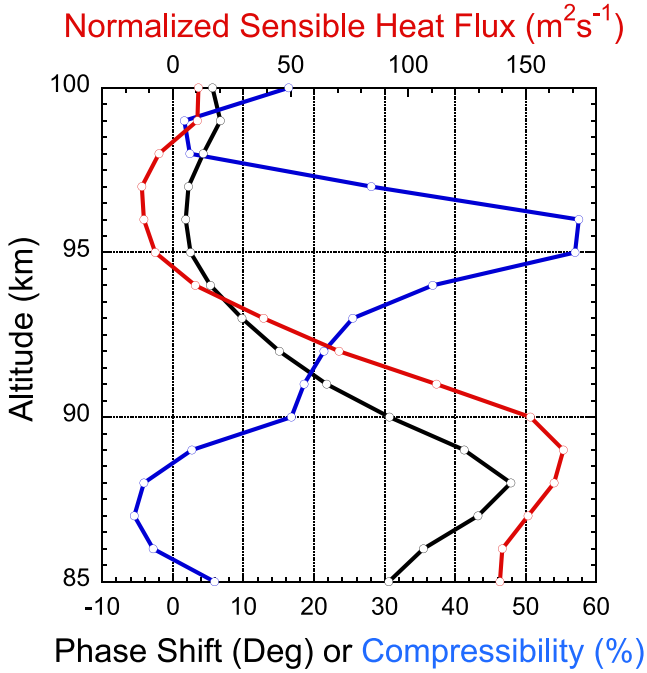

Figure 1. Profiles of the normalized sensible heat flux ($-\frac{g}{N^2}\frac{\overline{w'T'}}{\overline{T}}$, red curve, m^2s^{-1}), which may be regarded as a proxy for the strength of wave dissipation, the mean phase shift between w' and T' ($\overline{\Delta\phi_{w'T'}}$, black curve, degrees), and the mean normalized compressibility parameter ($\frac{\overline{\psi}}{1-\tilde{\kappa}}$, blue curve, %) that were derived from the Starfire Optical Range, NM data set and are tabulated in Table 2.

The mean phase shift ($\overline{\Delta\phi_{w'T'}}$) and compressibility profiles ($\overline{\psi}$) are then calculated from the derived K_E profile, and the measured sensible heat flux profile using Equations 27, 32 and 36.

$$\overline{\Delta\phi_{w'T'}} \simeq sin^{-1}\left\{-\frac{g}{N^2}\frac{\overline{w'\theta'}}{\overline{\theta}}\frac{\left(\Gamma_{ad}+\partial\overline{T}/\partial z\right)^2}{\varepsilon(q)\,fVar\left(T'\right)}\exp\left[Var\left(\Delta\phi_{w'T'}\right)/2\right]\right\} \quad (37)$$

$$\overline{\psi} \simeq \tilde{\kappa}\xi_{inst}\left\{2+\frac{\left[\left(\frac{C_p}{R}-1\right)K_E+K_{zz}+K_H^m\right]}{-\frac{g}{N^2}\frac{\overline{w'\theta'}}{\overline{\theta}}}\right\}-\tilde{\kappa} \quad (38)$$

To solve Equation 37 for the mean phase shift associated with dissipation, we need to know the variance of $\Delta\phi_{w'T}$, which is dominated by the variance of the much larger phase shift between w' and T' predicted by the polarization relations. We assume the standard deviation is 26.7° = 0.466 rad, which is the value measured by Lu et al. (2017) for the mesopause region above Boulder, CO. The mean phase shift profile for the SOR data set is tabulated in Table 2 and plotted versus altitude in Figure 1 ($\overline{\Delta\phi_{w'T'}}$, black curve). Also plotted is the normalized sensible heat flux ($-\frac{g}{N^2}\frac{\overline{w'T'}}{\overline{T}}$, red curve), which serves as a proxy for dissipation where large (small) values correspond to regions of strong (weak) dissipation. The phase shift varies from a low value of 1.8° at 96 km, where the normalized sensible heat flux is slightly negative, to a high value of 47.9° at 88 km, where the normalized heat flux is large and positive. The mean value between 85 and 100 km is 19°, which is much larger than the 2.6° mean derived by Lu et al. (2017) from observations of quasi-monochromatic waves. We believe this is credible because the waves are experiencing significant dissipation below 92 km, as indicated by the large positive values for the normalized sensible heat and potential temperature fluxes tabulated in Table 2, while above 92 km the dissipation is much weaker. We speculate that the approach employed by Lu et al. (2017) to identify and characterize individual quasi-monochromatic waves is biased toward the large amplitude, weakly dissipating waves for which the phase shift is small. Thus, we believe the estimated phase shifts in Table 2 are qualitatively consistent with the measured sensible heat and potential temperature fluxes. However, the largest values between 85 and 91 km, where dissipation is strongest, probably exceed the range where the modified polarization relations, derived in Chu et al. (2022), are applicable. Recall that these researchers simply added phase shifts, between w' and T' and w' and p', to the polarization relations derived by Vadas (2013) for non-dissipating waves. For strong dissipation it's likely the magnitudes as well as the phase shifts of the polarization relations change, in which case (27) and (32) may not be accurate for the larger values of $\overline{\Delta\phi_{w'T'}}$.

To solve Equation 38 for the mean compressibility of the wave fluctuations ($\overline{\psi}$), we assume that below 100 km K_H^m is negligible in comparison to K_E and K_{zz}. Because the eddy diffusivity profile was not measured at SOR, we employ a Gaussian model for K_{zz} that exhibits its maximum value (150 m^2/s) at 85 km, where the measured downward heat flux is large, which suggests this is a region of strong wave dissipation. The rms width of the profile was chosen as 5 km. Alternatively, because the heat fluxes are closely related to wave dissipation and turbulence, we could have used the scaled heat fluxes $\left(-\frac{g}{N^2}\frac{\overline{w'\theta'}}{\overline{\theta}}\ or\ -\frac{g}{N^2}\frac{\overline{w'T'}}{\overline{T}}\right)$, as a proxies for K_{zz}. Since the results are similar, here for simplicity, we present only the results for the Gaussian model. The mean compressibility profile for the wave spectrum, normalized by the fully compressible value $\left(1-\tilde{k}\right)$, is tabulated in Table 2 and plotted in Figure 1 ($\frac{\overline{\psi}}{1-\tilde{\kappa}}$, blue curve). Below 92 km in the region of strong dissipation, the normalized compressibility parameter is near zero, suggesting that the wave fluctuations are nearly incompressible. The normalized compressibility is maximum (57.5%) at 96 km, the same altitude where the phase shift associated with dissipation is minimum (1.8°) and the sensible heat flux is nearly minimum. In this region of weak dissipation, as

expected, the wave fluctuations are compressible, but they are clearly not fully compressible (100%). The mean value between 85 and 100 km is 17.4%. This demonstrates that the spectrum of wave-induced fluctuations is moderately, but not fully, compressible in the same region where the phase shift associated with dissipation is small (but not negligible) and is nearly incompressible where dissipation, $\overline{\Delta\phi_{w'T'}}$, $\left|\overline{w'T'}\right|$, and K_{zz} are largest. This is not surprising given the dependence of $\overline{\Delta\phi_{w'T'}}$ and $\overline{\psi}$ on the normalized potential temperature flux and K_{zz} exhibited by Equations 37 and 38.

7. Implications for Parameterizing Wave Mixing in Global Models

To incorporate mixing by non-breaking waves into global chemistry-climate models, it is necessary to compute the key transport parameters defined in Table 1, from data provided by the gravity wave, turbulence, and molecular diffusion modules employed by the models. From a practical standpoint, this involves estimating the potential temperature flux, induced by the unresolved, parameterized waves, in terms of either the mean phase shift $\left(\overline{\Delta\phi_{w'T'}}\right)$ caused by dissipation or the mean compressibility $(\overline{\psi})$ of the spectrum of waves. In the real atmosphere, the vertical Stokes drift velocity, associated with upwardly propagating waves, transports the background atmosphere upward. To maintain continuity, there must be descent elsewhere (Coy et al., 1986). Observational data like that obtained at SOR will include the impact of Stokes drift. Most global chemistry-climate models, parameterize unresolved waves, but do not include the Stokes drift induced by those waves. Without Stokes drift, wave mixing of heat and inert constituents may be modeled as pure diffusion processes where the total constituent and potential temperature fluxes, induced by waves, turbulence, and molecular diffusion, are.

$$F_C^z \simeq -\overline{\rho}_C\left(K_{Wave} + K_{zz} + K_C^m\right)\frac{\left(1+\xi_{inst}\right)}{\left(\overline{\rho}_C/\overline{\rho}_A\right)}\frac{\partial\left(\overline{\rho}_C/\overline{\rho}_A\right)}{\partial z} \tag{39}$$

$$F_\theta^z \simeq -\overline{\theta}\left(K_H + K_{zz} + K_H^m\right)\frac{\left(1+\xi_{inst}\right)}{\overline{\theta}}\frac{\partial\overline{\theta}}{\partial z} \tag{40}$$

In the absence of Stokes drift, the effective wave-induced thermal diffusivity is obtained directly from Fick's First Law of Diffusion using Equations 32 and 36.

$$K_H = -\frac{\overline{w'\theta'}}{\partial\overline{\theta}/\partial z} = -\frac{g}{N^2}\frac{\overline{w'\theta'}}{\overline{\theta}} \simeq \begin{cases} -\varepsilon(q)\exp\left[-\mathrm{Var}\left(\Delta\phi_{w'T'}\right)/2\right]\sin\left(\overline{\Delta\phi_{w'T'}}\right)\dfrac{f\mathrm{Var}\left(T'\right)}{\left(\Gamma_{ad}+\partial\overline{T}/\partial z\right)^2} \\ \dfrac{-\tilde{\kappa}\xi_{inst}}{\left(\overline{\psi}+\tilde{\kappa}-2\tilde{\kappa}\xi_{inst}\right)}\left[\left(\dfrac{C_p}{R}-1\right)K_E + K_{zz} + K_H^m\right] \end{cases} \tag{41}$$

For the modeled atmosphere, K_H is much smaller than the value given by Equation 29 for the real atmosphere because the vertical heat diffusion is not required to balance the upward advective transport of heat caused by Stokes drift. K_{Wave} is unchanged but can now be expressed in terms of K_H by combining Equations 41 and 28. The thermal and constituent diffusivity profiles for the SOR data set, with and without Stokes drift, are plotted in Figure 2. The key wave mixing parameters for the modeled atmosphere, without Stokes drift, are summarized in Table 3.

Wave parameterization schemes in models like WACCM, generate a spectrum of waves in the troposphere, typically launched by orography, convection, and frontogenesis (e.g., Beres et al., 2005; Charron & Manzini, 2002). The parameterized wave amplitudes are calculated as the waves propagate upward through the background atmosphere into the thermosphere. K_{zz} is computed when a wave breaks, and the wave is then eliminated from the spectrum. K_H^m is also readily computed from model data (see Equation 26). The only parameters, which cannot be computed from this type of wave parametrization scheme, are the phase shifts between w' and T' caused by dissipation $\left(\Delta\phi_{w'T'}\right)$ and the mean compressibility of the wave spectrum $(\overline{\psi})$. These may be treated as tunable parameters with values selected to provide the best agreement with observations. To test the effectiveness of Equation 41, here we simply use the SOR mean values derived in Table 2, viz. $\overline{\Delta\phi_{w'T'}} = 19°$ and

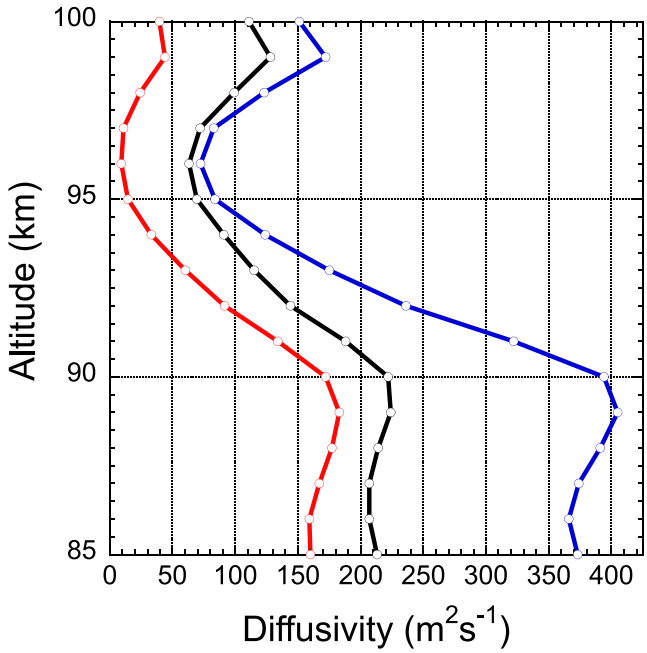

Figure 2. Plots of the wave-driven thermal diffusivity profiles (K_H) that were derived from the Starfire Optical Range (SOR), NM data set, with Stokes Drift (blue curve, Equation 29 & Table 2), and without Stokes Drift (red curve, Equation 41 & Table 4). Plot of the wave-driven constituent diffusivity profile (K_{Wave}) that was derived from the SOR data set (black curve, Equations 28 and 41 & Table 2).

$\overline{\psi/(1-\tilde{\kappa})} = 17.4\%$. As noted previously, because the K_{zz} profile was not measured at SOR, we employ a Gaussian model (Table 2).

We focus on the K_H profile because for the modeled atmosphere, K_{Wave} is directly related to the calculated values of K_E (see Equation 32) and the predicted values of K_H (see Table 3). The measured and predicted K_H profiles are tabulated in Table 4 and plotted in Figure 3. The mean differences are small, which indicates that the thermal diffusivity formulas given by the right-hand-sides of Equation 41 are scaled reasonably well. However, the large root-mean-square (RMS) difference between the measured and predicted profile for $\overline{\Delta\phi_{w'T'}} = 19°$, shows that parameterizing K_H by using a fixed phase shift is rather crude. In contrast, given the smaller RMS difference for the $\overline{\psi/(1-\tilde{\kappa})} = 17.4\%$ profile, parameterizing K_H using a fixed value for compressibility appears promising. The major difference between the measured and predicted profiles occurs below 90 km, where the wave dissipation is especially strong, and the normalized compressibility of the wave-driven fluctuations is considerably smaller than the mean value (Table 2).

As an alternative to employing a fixed value for $\overline{\psi}$ in Equation 36, we consider a proxy for the normalized potential temperature flux given by

$$-\frac{g}{N^2}\frac{\overline{w'\theta'}}{\overline{\theta}} \simeq Proxy = \eta\tilde{\kappa}\xi_{inst}\left[\left(\frac{C_p}{R}-1\right)K_E + K_{zz} + K_H^m\right], \qquad (42)$$

where η is chosen to provide the best fit to the measured profile. This is equivalent to replacing $\left(\overline{\psi}+\tilde{\kappa}-2\tilde{\kappa}\xi_{inst}\right)^{-1}$ in Equation 36 with a constant, rather than replacing $\overline{\psi}$. The best fit to the SOR data is obtained for $\eta \simeq 8.39$, in which case the mean difference between the measured and estimated profiles is $-7.6\ m^2/s$ and the rms difference is $30.9\ m^2/s$. The resulting proxy profile is tabulated in Table 4 and plotted in Figure 3 (black curve). This is clearly a better option for the SOR data

Table 3
Summary of Key Wave Mixing Parameters for the Modeled Atmosphere w/o Stokes Drift

Parameter	Formula[a,b]	Eq. #
Total Vertical Constituent Flux for Chemically Inert Species	$F_C^z \simeq -\overline{\rho}_C\left(K_{Wave}+K_{zz}+K_C^m\right)\frac{(1+\xi_{inst})}{(\overline{\rho}_C/\overline{\rho}_A)}\frac{\partial(\overline{\rho}_C/\overline{\rho}_A)}{\partial z}$	(39)
Total Vertical Flux of Potential Temperature	$F_\theta^z \simeq -\overline{\theta}\left(K_H+K_{zz}+K_H^m\right)\frac{(1+\xi_{inst})}{\overline{\theta}}\frac{\partial\overline{\theta}}{\partial z}$	(40)
Equivalent Diffusivity for Wave Energy Flux	$K_E = \frac{g}{N^2}\frac{R}{C_p}\frac{\overline{w'p'}}{\overline{p}} \simeq \beta(s,q)(1-2\alpha_{down})\frac{\Gamma_{ad}}{\overline{T}}\sqrt{\frac{Var(T')}{Var(\partial T'/\partial z)}}\frac{fVar(T')}{(\Gamma_{ad}+\partial\overline{T}/\partial z)^2}$	(32)
Wave-Induced Constituent Diffusivity	$K_{Wave} \simeq \frac{g}{N^2}\frac{\overline{w'\rho_A'}}{\overline{\rho}_A} = \left(\frac{C_p}{R}-1\right)K_E + K_H$	(28) & (41)
Wave-Induced Thermal Diffusivity	$K_H = -\frac{\overline{w'\theta'}}{\partial\overline{\theta}/\partial z} = -\frac{g}{N^2}\frac{\overline{w'\theta'}}{\overline{\theta}}$	(41)
Wave-Induced Vertical Flux of Sensible Heat	$\frac{g}{N^2}\frac{\overline{w'T'}}{\overline{T}} = K_E + \frac{g}{N^2}\frac{\overline{w'\theta'}}{\overline{\theta}}$	(30)
Wave-Induced Vertical Flux of Potential Temperature	$\frac{g}{N^2}\frac{\overline{w'\theta'}}{\overline{\theta}} = \frac{g}{N^2}\left(\frac{\overline{w'T'}}{\overline{T}} - \frac{R}{C_p}\frac{\overline{w'p'}}{\overline{p}}\right)$	(32)
		(36)
	$= \begin{cases} -\varepsilon(q)\exp\left[-Var\left(\Delta\phi_{w'T'}\right)/2\right]\sin\left(\overline{\Delta\phi_{w'T'}}\right)\dfrac{fVar\left(T'\right)}{\left(\Gamma_{ad}+\partial\overline{T}/\partial z\right)^2} \\ \dfrac{-\tilde{\kappa}\xi_{inst}}{\left(\overline{\psi}+\tilde{\kappa}-2\tilde{\kappa}\xi_{inst}\right)}\left[\left(\frac{C_p}{R}-1\right)K_E + K_{zz} + K_H^m\right] \end{cases}$	

[a]β(s,q) and ε(q) are defined, respectively, by (A-7) and (15) in Chu et al. (2022). [b]ξ_{inst} is defined by Equation 13, ψ by Equation 18, and $\tilde{\kappa}$ by Equation 20 in this paper.

Table 4
Measured and Estimated Thermal Diffusivity Profiles Induced by Waves at Starfire Optical Range, NM Without Stokes Drift

Altitude (km)	Measured K_H(m^2s^{-1})[a] $K_H = -\frac{g}{N^2}\frac{\overline{w'\theta'}}{\overline{\theta}}$ Equations 27 and 30	Estimated K_H(m^2s^{-1}) $\overline{\Delta\phi_{w'T'}} = 19°$ Equation 32	Estimated K_H(m^2s^{-1}) $\overline{\psi}/(1-\tilde{\kappa}) = 17.4\%$ Equation 36	Estimated K_H(m^2s^{-1}) Proxy $\eta \simeq 8.39$ Equation 42
100	39.6	103	61.6	63.8
99	44.0	103	39.3	51.3
98	24.2	87.3	21.5	35.7
97	11.1	78.7	18.0	33.0
96	9.2	79.7	23.1	41.4
95	14.5	89.0	38.4	59.6
94	33.0	97.3	69.3	83.6
93	60.3	96.4	98.8	101
92	91.6	94.8	135	123
91	134	97.3	184	148
90	172	91.5	177	156
89	183	74.6	116	144
88	177	64.7	80.9	133
87	167	69.0	66.5	131
86	159	74.1	67.3	136
85	160	85.6	93.8	161
Mean Difference		**−5.8**	**−11.8**	**−7.6**
RMS Difference		**73.6**	**53.0**	**30.9**

[a]Table S1, Supporting Information, This paper.

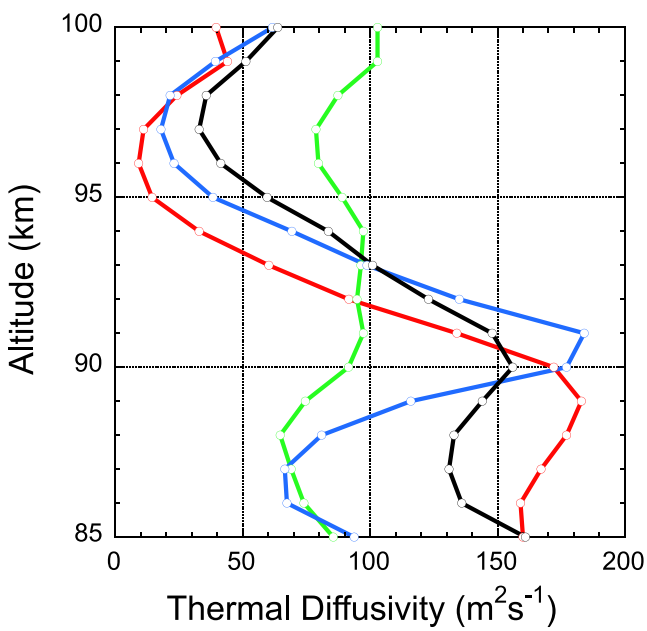

Figure 3. Wave-driven thermal diffusivity (K_H) profile (red curve) derived from the Starfire Optical Range, NM data set without Stokes Drift. Estimated K_H profiles calculated by assuming a fixed value of $\overline{\Delta\phi_{w'T'}} = 19°$ (green curve), a fixed value of $\overline{\psi}/(1-\tilde{\kappa}) = 17.4\%$ (blue curve), and by using the proxy given by Equation 42 with $\eta \simeq 8.39$ (black curve). The profiles are tabulated in Table 4.

set. Unfortunately, because of the lack of flux observations outside the mesopause region, it is not clear how applicable Equation 42 is in the thermosphere above 100 km or in the mesosphere and stratosphere below 85 km. Hence, we suggest treating η as a tunable parameter that varies slowly with height and is adjusted to provide the best fit between key model predictions and observations.

Each of the estimated K_H profiles depends on the instability parameter ξ_{inst} which, ideally, is computed from the lapse rate fluctuations (see Equation 13). The value of ξ_{inst} depends strongly on the vertical wavenumber (m) spectrum of the temperature fluctuations. If the wave parameterization scheme employed by a global model includes waves that are representative of the widely observed temperature m-spectrum, then ξ_{inst} may be computed directly from these parameterized waves. Otherwise, the instability parameter should be computed from the temperature fluctuation variance of the parameterized waves by employing an appropriate theoretical model for the m-spectrum. This latter approach was used by Guarino et al. (2024) to compute ξ_{inst} from data provided by the wave parameterization scheme in the WACCM (see Appendix A, Guarino et al., 2024).

Superimposed on the coherent motion imparted to the atmosphere by an atmospheric wave are the random thermal motions of individual molecules (molecular viscosity), and the larger-scale random motions imparted by turbulence (eddy viscosity) and the full spectrum of waves. The diffusion associated with these multi-scale processes degrades the organized bulk motion associated with an individual wave and leads to attenuation of the wave. Damping of wave amplitudes by the viscosity of the atmosphere was

first examined by Hines (1960) and then extended by Pitteway and Hines (1963) to include both viscous and conductive dissipation. Later Weinstock (1976, 1990) showed that atmospheric mixing by waves and turbulence also damps the wave amplitudes. Models like WACCM include wave damping by molecular viscosity and thermal conduction, but not diffusive damping by turbulence and waves (Appendix, Garcia et al., 2007). To derive the correct temperature fluctuation variances from the parameterized waves in the WACCM scheme, it was necessary for Guarino et al. (2024) to incorporate diffusive damping by waves and turbulence. Their approach can also be applied to other models, which don't currently include diffusive damping, by using the K_{zz} that is computed when waves dissipate or break, and the wave diffusivities derived here from theory.

The important Prandtl ($Pr = K_M/K_H$) and Schmidt ($Sc = K_M/K_{Mass}$) numbers are typically assumed to be free parameters in the wave schemes employed by global models (e.g., Appendix, Garcia et al., 2007), where K_M, K_H and K_{Mass} are the effective momentum, thermal, and mass diffusion coefficients of the parameterized wave spectrum. As shown by Liu (2009), K_M and K_H can be deduced from knowledge of the wave-driven momentum flux and potential temperature flux profiles and used to calculate the Prandtl number profile. Momentum fluxes of the parameterized gravity waves are computed in the model wave schemes (e.g., Appendix, Garcia et al., 2007) from which K_M can be deduced. Both K_H and $K_{Mass} = H_A \frac{\overline{w'\rho'_A}}{\bar{\rho}_A} = \frac{N^2 H_A}{g} K_{Wave}$ can be computed from the theory described in this paper, so it should be possible to estimate Pr and Sc for the parameterized waves, thereby eliminating these free parameters.

Currently, global models with parameterized gravity waves do not consider the effects of secondary and higher-order gravity waves that are generated when primary gravity waves break. These waves can propagate both upward and downward and their impact on species and heat transport depends on the vertical propagation direction. Lidar observations of the mesopause region at McMurdo, have observed these higher-order waves and assessed their effects (Chu et al., 2022; Vadas et al., 2018). Recent modeling studies by Becker and Vadas (2018) showed that higher-order waves are required to produce the correct large-scale flow in the winter mesosphere. Furthermore, Becker et al. (2020) showed that mixing and species transport by higher-order waves affects the morphology of the OH airglow layer near the mesopause. In the theory presented here, higher-order and other downward propagating waves, impact mixing by enhancing the mean mixing ratio gradients through the parameter ξ_{inst} and by affecting the fraction of downward propagating wave energy α_{down}, which in turn affects K_E, K_H, and K_{Wave}. Although the wave transport theory can accommodate higher-order waves, as well as downward propagating waves caused by ducting and reflections from above, to properly calculate the dominant transport effects, it may be important for future modeling schemes to include higher-order and other downward propagating waves in the parameterized wave spectrum. Finally, existing models do not include chemical transport of reactive species, which arises from wave perturbations that modulate of their chemical reactions. Chemical transport can be important for some upper atmospheric species (e.g., Gardner, 2018; Gardner & Liu, 2016).

The expressions for constituent and thermal fluxes were developed by assuming that the unperturbed species and atmospheric densities were horizontally homogeneous, which is a customary approximation employed in most gravity wave schemes applied to conventional global-chemistry models. In Appendix C, we show how the theory can be modified to include the contributions to the vertical species flux arising from horizontal inhomogeneities. These contributions may be important for high-resolution models that can resolve waves with horizontal wavelengths of a few hundred kms.

8. Summary and Conclusions

This study builds upon prior work by demonstrating that wave compressibility and Stokes drift can have a significant impact on the wave-driven vertical transport of heat and constituents, especially in the mesopause region. In the MLT the effective diffusivities for potential temperature (K_H) and constituents (K_{Wave}) are generally much larger than the eddy diffusivity (K_{zz}) and can exceed several hundred m^2/s. Furthermore, wave-driven, eddy, and molecular diffusion are all enhanced in the presence of gravity waves by up to 50% or more, because the average vertical gradients of potential temperature and constituent mixing ratios are amplified by the wave fluctuations. K_H and K_{Wave} can be expressed in terms of the wave energy $(\overline{w'p'})$ and sensible heat $(\overline{w'T'})$ fluxes. Both diffusivities can be negative in regions where the wave spectrum is dominated by downward propagating waves so that $\overline{w'p'} < 0$, and in regions where the spectrum is dominated by upwardly propagating, weakly dissipating waves with fast

vertical phase speeds so that $0 \ll \overline{w'T'}$ (Chu et al., 2022). Unless the molecular and eddy diffusivities are large enough to counteract the negative K_H or K_{Wave} values, it is possible for waves to transport heat and constituents against the potential temperature and mixing ratio gradients. Finally, we used the gravity wave polarization relations and the advection-diffusion equation to express K_H and K_{Wave} in terms of parameters that are readily derived from the predictions of global chemistry-climate models. These latter results may now be used, in combination with the predicted chemical fluxes of important reactive species (Gardner, 2018; Gardner & Liu, 2016; Walterscheid & Schubert, 1989), to more fully account for the unresolved wave transport in global models.

Although the theory compares favorably with mesopause region observations at midlatitudes, the analysis is general and can be used to estimate wave transport at any altitude and location. All that is needed are the profiles of the temperature of the background atmosphere $\overline{T}(z)$, the temperature and lapse rate fluctuation variances, $Var[T'(z)]$ and $Var[-\partial T'(z)/\partial z]$, the eddy diffusivity $K_{zz}(z)$, and the molecular diffusivities for heat $K_H^m(z)$ and constituents $K_C^m(z)$. The transport parameters, K_H, K_{Wave}, and ξ_{inst}, can be computed from these profiles. The results show that it is important to include unresolved wave transport by nonbreaking waves in atmospheric models, especially in the upper atmosphere where wave-driven diffusion can reduce thermosphere densities by enhancing the downward transport of O into the mesopause region (e.g., Gardner, 2018; Pilinski & Crowley, 2015; Qian et al., 2009), alter mesopause region temperatures by, among other effects, transporting CO_2 upward thereby enhancing radiative cooling, and speed the transport of cosmic dust ablation products into the lower atmosphere (Guarino, et al., 2024). Observations of temperatures, winds, and turbulence, made throughout the atmosphere, in combination with the expressions derived here, can now be used to assess the significance of wave transport at all altitudes and to model its effects.

Appendix A: Solutions for δ_C and $\overline{w'\delta_C}$

We approximate δ_C by its first order-perturbation solution to Equation 9, where for completeness, we consider the total atmospheric diffusivity instead of just K_{Wave}. To simplify the derivation, we assume that the altitude variations of the total diffusivity $\left(K_{Wave} + K_{zz} + K_C^m\right)$ are negligible in comparison to the altitude variations of ρ'_C and we neglect the fluctuations in K_C^m associated with the wave-induced fluctuations in pressure and temperature, which are not important below 100 km. Under these conditions, Equation 9 reduces to

$$\frac{\partial \delta_C}{\partial t} \simeq \frac{\left(K_{Wave} + K_{zz} + K_C^m\right)}{\overline{\rho}_C}\left\{\frac{\rho'_C}{\overline{\rho}_C}\frac{\partial}{\partial z}\left[\overline{\rho}_A \frac{\partial}{\partial z}\left(\frac{\overline{\rho}_C}{\overline{\rho}_A}\right)\right] - \frac{\partial}{\partial z}\left[\rho_A \frac{\partial}{\partial z}\left(\frac{\rho_C}{\rho_A}\right)\right]'\right\}. \tag{A1}$$

We also assume that the effective vertical diffusion velocity $\left(K_{Wave} + K_{zz} + K_C^m\right)m$ is much slower than the vertical phase velocity of the wave (ω/m) and ignore those terms that are in phase quadrature with w', in which case Equation A1 simplifies to

$$\frac{\partial \delta_C}{\partial t} \simeq -\left(K_{Wave} + K_{zz} + K_C^m\right)\frac{\partial^2}{\partial z^2}\left(\frac{\rho'_C}{\overline{\rho}_C} - \frac{\rho'_A}{\overline{\rho}_A}\right)$$

$$\simeq \left(K_{Wave} + K_{zz} + K_C^m\right)\left[\frac{\partial^2}{\partial z^2}\delta_C + \frac{1}{\left(\overline{\rho}_C/\overline{\rho}_A\right)}\frac{\partial\left(\overline{\rho}_C/\overline{\rho}_A\right)}{\partial z}\frac{\partial^2}{\partial z^2}\zeta\right]. \tag{A2}$$

Transforming Equations A1 and A2 into the complex 2D-(ω,m) Fourier domain and solving for $\delta_C(\omega,m)$ yields

$$\delta_C(\omega,m) \simeq -\left(K_{Wave} + K_{zz} + K_C^m\right)\frac{1}{\left(\overline{\rho}_C/\overline{\rho}_A\right)}\frac{\partial\left(\overline{\rho}_C/\overline{\rho}_A\right)}{\partial z}\frac{m^2}{i\omega}\zeta(\omega,m), \tag{A3}$$

where from Equations 16 and 21 in this paper, and Equation B-11 in Vadas (2013), the solution for $\zeta(\omega,m)$ when $\lambda_z << 176$ km, is

$$\zeta(\omega,m) \simeq \frac{w'(\omega,m)}{i\omega} \simeq \frac{T'(\omega,m)}{\left(\Gamma_{ad} + \frac{\partial \overline{T}}{\partial z}\right)}. \tag{A4}$$

Multiplying Equation A3 by the complex conjugate of $w'(\omega,m)$, taking the expectation, and then computing the inverse Fourier transform, we obtain the result.

$$\overline{w'\delta_C} \simeq \left(\mathrm{K_{Wave}} + \mathrm{K_{zz}} + \mathrm{K_C^m}\right) \frac{\xi_{inst}}{\left(\overline{\rho}_\mathrm{C}/\overline{\rho}_\mathrm{A}\right)} \frac{\partial\left(\overline{\rho}_\mathrm{C}/\overline{\rho}_\mathrm{A}\right)}{\partial \mathrm{z}} \tag{A5}$$

If we are only interested in the impact of wave-induced diffusion, then $\overline{w'\delta_C}$ is given by Equation A5 with $K_{zz} = K_C^m = 0$, which is identical to Equation 12.

Appendix B: Solutions for δ_θ and $\overline{w'\delta_\theta}$

In the absence of heat sources and sinks, potential temperature is a conserved quantity that is governed by the advection-diffusion equation for heat transfer.

$$\frac{\partial\theta}{\partial \mathrm{t}} + \nabla\cdot\left(\underline{\mathrm{V}}\theta\right) = \nabla\cdot\left[\left(\mathrm{K_H} + \mathrm{K_{zz}} + \mathrm{K_H^m}\right)\nabla\theta\right] \simeq \frac{\partial}{\partial z}\left[\left(\mathrm{K_H} + \mathrm{K_{zz}} + \mathrm{K_H^m}\right)\frac{\partial\theta}{\partial z}\right] \tag{B1}$$

Because of the similarity to Equation 4, we use an approach to solve for $\overline{w'\theta'}$ that is like the one used to solve for the species flux. The potential temperature is modeled as follows,

$$\theta = \mathrm{e}^{-\delta_\theta}\theta_0 \tag{B2}$$

where θ_0 is the potential temperature, perturbed by gravity waves in the absence of diffusion, while δ_θ accounts for the additional impact of molecular diffusion of heat and atmospheric mixing by waves and turbulence. By substituting Equation B2 into Equation B1 we find that δ_θ and θ_0 are solutions to the following differential equations.

$$\frac{\partial\delta_\theta}{\partial \mathrm{t}} = -\frac{1}{\theta}\frac{\partial}{\partial \mathrm{z}}\left[\left(\mathrm{K_H} + \mathrm{K_{zz}} + \mathrm{K_H^m}\right)\frac{\partial\theta}{\partial \mathrm{z}}\right] - \underline{\mathrm{V}}'\cdot\nabla\delta_\theta \tag{B3}$$

$$\frac{\partial\theta_0}{\partial \mathrm{t}} + \nabla\cdot\left(\underline{\mathrm{V}}\theta_0\right) = 0 \tag{B4}$$

The total vertical flux of potential temperature is

$$F_\theta^z = \overline{w'\theta'} - \overline{\theta}\left(\mathrm{K_{zz}} + \mathrm{K_H^m}\right)\frac{1}{\overline{\theta}}\frac{\partial\overline{\theta}}{\partial z} = \overline{w'\theta_0} - \overline{\theta}\,\overline{w'\delta_\theta} - \overline{\theta}\left(\mathrm{K_{zz}} + \mathrm{K_H^m}\right)\frac{1}{\overline{\theta}}\frac{\partial\overline{\theta}}{\partial z}, \tag{B5}$$

where the first term on the right-hand-side of Equation B5 is the wave-induced flux in the absence of molecular and eddy diffusion, which includes the contributions from Stokes drift and wave-mixing.

$$\overline{w'\theta_0} = \overline{\theta}\frac{\overline{w'\rho_A'}}{\overline{\rho}_A} - K_H\frac{\partial\overline{\theta}}{\partial z} \tag{B6}$$

The last term in Equation B5 is the contribution from molecular and turbulent diffusion, in the absence of waves, while the middle term is the additional diffusive flux associated with wave perturbations of the total heat diffusion.

To solve for $\overline{w'\delta_\theta}$, we approximate δ_θ by the first-order perturbation solution to Equation B3, assume the altitude variations of $\left(\mathrm{K_H} + \mathrm{K_{zz}} + \mathrm{K_H^m}\right)$ are negligible in comparison to the variations of θ', neglect the wave-induced fluctuations of $\mathrm{K_H^m}$, and also neglect terms that are in phase quadrature with w', so that Equation B3 simplifies to

$$\frac{\partial\delta_\theta}{\partial \mathrm{t}} \simeq -\left(\mathrm{K_H} + \mathrm{K_{zz}} + \mathrm{K_H^m}\right)\frac{\partial^2}{\partial z^2}\left(\frac{\theta'}{\overline{\theta}}\right). \tag{B7}$$

We apply the same approach used to solve for δ_C in Appendix A, recognizing that the effective vertical velocity of heat diffusion, $\left(K_H + K_{zz} + K_H^m\right) m$, is much slower than the vertical phase velocity of the wave (ω/m). The result for $\overline{w'\delta_\theta}$ is.

$$\overline{w'\delta_\theta} \simeq \left(K_H + K_{zz} + K_H^m\right) \frac{1}{\overline{\theta}} \frac{\partial \overline{\theta}}{\partial z} \frac{Var\left(\partial T'/\partial z\right)}{\left(\Gamma_{ad} + \partial \overline{T}/\partial z\right)^2} = \left(K_H + K_{zz} + K_H^m\right) \frac{\xi_{inst}}{\overline{\theta}} \frac{\partial \overline{\theta}}{\partial z} \tag{B8}$$

Substituting Equations B6 and B8 into Equation B5 gives the final expression for the total vertical flux of potential temperature.

$$F_\theta^z \simeq \overline{\theta} \overline{\frac{w'\rho_A'}{\overline{\rho}_A}} - \overline{\theta}\left(K_H + K_{zz} + K_H^m\right) \frac{\left(1 + \xi_{inst}\right)}{\overline{\theta}} \frac{\partial \overline{\theta}}{\partial z} \tag{B9}$$

Appendix C: Impact of Horizontal Inhomogeneities

We consider the impact of horizontal inhomogeneities in the unperturbed species profile by modeling the perturbed species and atmospheric densities as

$$\rho_C(x,y,z,t) = e^{-\delta_C - \chi} \rho_{C0}\left(x - \zeta_x, y - \zeta_y, z - \zeta_z\right) \tag{C1}$$

$$\rho_A(x,y,z,t) = e^{-\chi} \rho_{A0}\left(x - \zeta_x, y - \zeta_y, z - \zeta_z\right). \tag{C2}$$

The wave parameters ζ_x,ζ_y, and ζ_z are the vertical and horizontal displacements imparted to the unperturbed species profile by the wave perturbations, which are solutions to the following partial differential equations,

$$\frac{\partial \zeta_x}{\partial t} = u' - \underline{V}' \cdot \nabla \zeta_x \tag{C3}$$

$$\frac{\partial \zeta_y}{\partial t} = v' - \underline{V}' \cdot \nabla \zeta_y \tag{C4}$$

$$\frac{\partial \zeta_z}{\partial t} = w' - \underline{V}' \cdot \nabla \zeta_z \tag{C5}$$

where $u' \simeq w' \frac{N}{\omega} sin\, \phi_{az}$ and $v' \simeq w' \frac{N}{\omega} cos\, \phi_{az}$ are, respectively, the zonal and meridional wind perturbation, where ϕ_{az} is the azimuth angle of the wave propagation direction and, as before, χ and δ_C are solutions to Equations 8 and 9. The vertical transport velocity of a species, defined as the vertical flux divided by the mean species density, is given by

$$\overline{\frac{w'\rho_C'}{\overline{\rho}_C}} = \overline{\frac{w'\rho_A'}{\overline{\rho}_A}} - \overline{w'\delta_C} - \overline{\frac{w'\zeta_x}{\left(\overline{\rho}_C/\overline{\rho}_A\right)}} \frac{\partial\left(\overline{\rho}_C/\overline{\rho}_A\right)}{\partial x} - \overline{\frac{w'\zeta_y}{\left(\overline{\rho}_C/\overline{\rho}_A\right)}} \frac{\partial\left(\overline{\rho}_C/\overline{\rho}_A\right)}{\partial y} - \overline{\frac{w'\zeta_z}{\left(\overline{\rho}_C/\overline{\rho}_A\right)}} \frac{\partial\left(\overline{\rho}_C/\overline{\rho}_A\right)}{\partial z}. \tag{C6}$$

The first-order perturbation solutions for ζ_x and ζ_y are.

$$\zeta_x \simeq \int_{-\infty}^{t} u' d\tau \tag{C7}$$

$$\zeta_y \simeq \int_{-\infty}^{t} v' d\tau \tag{C8}$$

By applying the gravity wave polarization relations and assuming the ω-spectra for the horizontal wind perturbations are proportional to ω^{-2}, we obtain

$$\overline{\mathrm{w}'\zeta_x} \simeq \frac{\overline{w'v'}}{2fln(N/f)} \tag{C9}$$

$$\overline{\mathrm{w}'\zeta_y} \simeq \frac{\overline{w'u'}}{2fln(N/f)}, \tag{C10}$$

where $\overline{w'u'}$ and $\overline{w'v'}$ are, respectively, the vertical fluxes of zonal and meridional momentum. The calculations leading to Equations C9 and C10 employed the Stokes decomposition of the gravity wave spectrum described by Vincent and Fritts (1987). Horizontal inhomogeneities can be neglected when the following conditions are satisfied,

$$\left|\frac{\overline{\mathrm{w}'\zeta_x}}{(\overline{\rho}_C/\overline{\rho}_A)}\frac{\partial(\overline{\rho}_C/\overline{\rho}_A)}{\partial x}\right| \simeq \left|\frac{\overline{w'v'}}{2fln(N/f)\,H_{Cx}}\right| \ll \left|\frac{\overline{\mathrm{w}'\rho_C{}'}}{\overline{\rho}_C}\right| \tag{C11}$$

$$\left|\frac{\overline{\mathrm{w}'\zeta_y}}{(\overline{\rho}_C/\overline{\rho}_A)}\frac{\partial(\overline{\rho}_C/\overline{\rho}_A)}{\partial y}\right| \simeq \left|\frac{\overline{w'u'}}{2fln(N/f)\,H_{Cy}}\right| \ll \left|\frac{\overline{\mathrm{w}'\rho_C{}'}}{\overline{\rho}_C}\right|, \tag{C12}$$

where H_{Cx} and H_{Cy} are the zonal and meridional scale lengths of ρ_C. At mesopause heights the wave-driven vertical transport velocities vary from a few to more than 10 cm/s, depending on the species and altitude (e.g., Chu et al., 2022; Gardner, 2018; Gardner & Liu, 2016), while the momentum fluxes range between about ±4 m^2s^{-2} (Figure 14, Gardner & Liu, 2007). At mid-latitudes Equations C11 and C12 are satisfied when H_{Cx} and H_{Cy} are equal to or larger than a few thousand km.

For high-resolution models, that can resolve waves with horizontal wavelengths of a few hundred kms, it may not be valid to ignore the vertical flux contributions arising from horizontal inhomogeneities. The current theory can accommodate those contributions by applying Equation C6 and recognizing that H_{Cx} and H_{Cy}, which are computed from the modeled background species profile, will include the effects of the resolved, higher resolution waves.

Data Availability Statement

The data employed to make the calculations tabulated in Tables 2 and 4 are contained in Table S1 of the Supporting Information to this paper and the references therein.

Acknowledgments
This work was partially supported by National Science Foundation grants AGS-2029162 and OPP-2110422.

References

Andrews, D. G., & McIntyre, M. E. (1978). On wave-action and its relatives. *Journal of Fluid Mechanics*, *89*(4), 647–664. https://doi.org/10.1017/S0022112078002785

Becker, E., Grygalashvyly, M., & Sonnemann, G. R. (2020). Gravity wave mixing effects on the OH*-layer. *Advances in Space Research*, *65*(1), 175–188. https://doi.org/10.1016/j.asr.2019.09.043

Becker, E., & Vadas, S. L. (2018). Secondary gravity waves in the winter mesosphere: Results from a high-resolution global circulation model. *Journal of Geophysical Research: Atmospheres*, *123*(5), 2605–2627. https://doi.org/10.1002/2017JD027460

Beres, J. H., Alexander, M. J., & Holton, J. R. (2004). A method of specifying the gravity wave spectrum above convection based on latent heating properties and background wind. *Journal of the Atmospheric Sciences*, *61*(3), 324–337. https://doi.org/10.1175/1520-0469(2004)061<0324:AMOSTG>2.0.CO;2

Beres, J. H., Garcia, R. R., Boville, B. A., & Sassi, F. (2005). Implementation of a gravity wave source spectrum parameterization dependent on the properties of convection in the whole atmosphere community climate model (WACCM). *Journal of Geophysical Research*, *110*(D10). https://doi.org/10.1029/2004JD005504

Carrillo-Sánchez, J. D., Nesvorny, D., Pokorny, P., Janches, D., & Plane, J. M. C. (2016). Sources of cosmic dust in the Earth's atmosphere. *Geophysical Research Letters*, *43*(23), 11979–11986. https://doi.org/10.1002/2016GL071697

Charron, M., & Manzini, E. (2002). Gravity waves from fronts: Parameterization and middle atmosphere response in a general circulation model. *Journal of the Atmospheric Sciences*, *59*(5), 923–941. https://doi.org/10.1175/1520-0469(2002)059<0923:GWFFPA>2.0.CO;2

Chu, X., Gardner, C. S., & Franke, S. J. (2004). Nocturnal thermal structure of the mesosphere and lower thermosphere region at Maui, Hawaii (20.7°N), and Starfire Optical Range, New Mexico (35°N). *Journal of Geophysical Research*, *110*(D9). https://doi.org/10.1029/2004JD004891

Chu, X., Gardner, C. S., Li, X., & Lin, C. Y.-T. (2022). Vertical transport of sensible heat and meteoric Na by the complete temporal spectrum of gravity waves in the MLT above McMurdo (77.84°S, 166.67°E), Antarctica. *Journal of Geophysical Research: Atmospheres*, *127*(16), e2021JD035728. https://doi.org/10.1029/2021JD035728

Coy, L., Fritts, D. C., & Weinstock, J. (1986). The Stokes drift due to vertically propagating internal gravity waves in a compressible atmosphere. *Journal of the Atmospheric Sciences*, *43*(22), 2636–2643. https://doi.org/10.1175/1520-0469(1986)043<2636:TSDDTV>2.0.CO;2

Eckermann, S. D., & Vincent, R. A. (1989). Falling sphere observations of anisotropic gravity wave motions in the upper stratosphere over Australia. *Pure and Applied Geophysics*, *130*(2–3), 509–532. https://doi.org/10.1007/BF00874472

Feng, W., Marsh, D. R., Chipperfield, M. P., Janches, D., Höffner, J., Yi, F., & Plane, J. M. C. (2013). A global atmospheric model of meteoric iron. *Journal of Geophysical Research: Atmospheres*, *118*(16), 9456–9474. https://doi.org/10.1002/jgrd.50708

Fritts, D. C., & Dunkerton, T. J. (1985). Fluxes of heat and constituents due to convectively unstable gravity waves. *Journal of Atmospheric Science*, *42*(6), 549–556. https://doi.org/10.1175/1520-0469(1985)042<0549:FOHACD>2.0.CO;2

Garcia, R. R., Marsh, D. R., Kinnison, D. E., Boville, B. A., & Sassi, F. (2007). Simulation of secular trends in the middle atmosphere, 1950–2003. *Journal of Geophysical Research*, *112*(D9). https://doi.org/10.1029/2006JD007485

Gardner, C. S. (2018). Role of wave-induced diffusion and energy flux in the vertical transport of atmospheric constituents in the mesopause region [Dataset]. *Journal of Geophysical Research: Atmospheres*, *123*(12), 6581–6604. https://doi.org/10.1029/2018JD028359

Gardner, C. S., Guo, Y., & Liu, A. Z. (2019). Parameterizing wave-driven vertical constituent transport in the upper atmosphere [Dataset]. *Earth and Space Science*, *6*, 904–913. https://doi.org/10.1029/2019EA000625

Gardner, C. S., & Liu, A. Z. (2007). Seasonal variations of the vertical fluxes of heat and horizontal momentum in the mesopause region at Starfire Optical Range, New Mexico [Dataset]. *Journal of Geophysical Research*, *112*(D9), D09113. https://doi.org/10.1029/2005JD006179

Gardner, C. S., & Liu, A. Z. (2010). Wave-induced transport of atmospheric constituents and its effect on the mesospheric Na layer. *Journal of Geophysical Research*, *115*(D20), D20302. https://doi.org/10.1029/2010JD014140

Gardner, C. S., & Liu, A. Z. (2016). Chemical transport of neutral atmospheric constituents by waves and turbulence: Theory and observations. *Journal of Geophysical Research: Atmospheres*, *121*(1), 494–520. https://doi.org/10.1002/2015JD023145

Gardner, C. S., Liu, A. Z., & Guo, Y. (2017). Vertical and horizontal transport of mesospheric Na: Implications for the mass influx of cosmic dust. *Journal of Atmospheric and Solar-Terrestrial Physics*, *162*, 192–202. https://doi.org/10.1016/j.jastp.2016.07.013

Gardner, C. S., & Shelton, J. D. (1985). Density response of neutral atmospheric layers to gravity wave perturbations. *Journal of Geophysical Research*, *90*(A2), 1745–1754. https://doi.org/10.1029/JA090iA02p01745

Gettelman, A., Mills, M. J., Kinnison, D. E., Garcia, R. R., Smith, A. K., Marsh, D. R., et al. (2019). The whole atmosphere community climate model version 6 (WACCM6). *Journal of Geophysical Research: Atmospheres*, *124*(23), 12380–12403. https://doi.org/10.1029/2019JD030943

Grygalashvyly, M., Becker, E., & Sonnemann, G. R. (2012). Gravity wave mixing and effective diffusivity for minor chemical constituents in the mesosphere/lower thermosphere. *Space Science Reviews*, *168*(1–4), 333–362. https://doi.org/10.1007/s11214-011-9857-x

Guarino, M.-V., Gardner, C. S., Feng, W., Funke, B., Garcia-Comas, M., Lopez-Puertas, M., et al. (2024). A novel gravity wave transport parametrization for global chemistry climate models: Description and validation. *Journal of Advances in Modeling Earth Systems*. https://doi.org/10.22541/essoar.169111440.01591117/v2

Guo, Y., & Liu, A. Z. (2021). Seasonal variation of vertical heat and energy fluxes due to dissipating gravity waves in the mesopause region over the Andes. *Journal of Geophysical Research: Atmospheres*, *126*(3), e2020JD033825. https://doi.org/10.1029/2020JD033825

Hickey, M. P., Walterscheid, R. L., & Philip, P. G. (2000). Secular variations of atomic oxygen in the mesopause region induced by transient gravity wave packets. *Geophysical Research Letters*, *27*(21), 3599–3602. https://doi.org/10.1029/2000GL011953

Hines, C. O. (1960). Internal atmospheric gravity waves at ionospheric heights. *Canadian Journal of Physics*, *38*(11), 1441–1481. https://doi.org/10.1139/p60-150

Hu, X., Liu, A. Z., Gardner, C. S., & Swenson, G. R. (2002). Characteristics of quasi-monochromatic gravity waves observed with lidar in the mesopause region at Starfire Optical Range, NM. *Geophysical Research Letters*, *29*(24), 2169. https://doi.org/10.1029/2002GL014975

Huang, W., Chu, X., Gardner, C. S., Carrillo-Sánchez, J. D., Feng, W., Plane, J. M. C., & Nesvorny, D. (2015). Measurements of the vertical fluxes of atomic Fe and Na at the mesopause: Implications for the velocity of cosmic dust entering the atmosphere. *Geophysical Research Letters*, *42*(1), 169–175. https://doi.org/10.1002/2014GL062390

Liu, A. Z. (2009). Estimate eddy diffusion coefficients from gravity wave vertical momentum and heat fluxes. *Geophysical Research Letters*, *36*(8). https://doi.org/10.1029/2009GL037495

Liu, A. Z., & Gardner, C. S. (2004). Vertical dynamical transport of mesospheric constituents by dissipating gravity waves. *Journal of Atmospheric and Solar-Terrestrial Physics*, *66*(3–4), 267–275. https://doi.org/10.1016/j.jastp.2003.11.002

Liu, H.-L. (2000). Temperature changes due to gravity wave saturation. *Journal of Geophysical Research*, *105*(D10), 12329–12336. https://doi.org/10.1029/2000JD900054

Liu, H.-L. (2021). Effective vertical diffusion by atmospheric gravity waves. *Geophysical Research Letters*, *48*(1), e2020GL091474s. https://doi.org/10.1029/2020GL091474

Lu, X., Chu, X., Li, H., Chen, C., Smith, J. A., & Vadas, S. L. (2017). Statistical characterization of high-to-medium frequency mesoscale gravity waves by lidar-measured vertical winds and temperatures in the MLT. *Journal of Atmospheric and Solar-Terrestrial Physics*, *162*, 3–15. https://doi.org/10.1016/j.jastp.2016.10.009

Marsh, D. R., Janches, D., Feng, W., & Plane, J. M. C. (2013). A global model of meteoric sodium. *Journal of Geophysical Research: Atmospheres*, *118*(19), 11442–11452. https://doi.org/10.1002/jgrd.50870

Nakamura, N. (2001). A new look at eddy diffusivity as a mixing diagnostic. *Journal of the Atmospheric Sciences*, *58*(24), 3685–3701. https://doi.org/10.1175/1520-0469(2001)

Pilinski, M. D., & Crowley, G. (2015). Seasonal variability in global eddy diffusion and the effect on neutral density. *Journal of Geophysical Research: Space Physics*, *120*(4), 3097–3117. https://doi.org/10.1002/2015JA021084

Pitteway, M. L. U., & Hines, C. O. (1963). The viscous damping of atmospheric gravity waves. *Canadian Journal of Physics*, *41*(12), 1935–1948. https://doi.org/10.1139/p63-194

Plane, J. M. C., Feng, W., & Dawkins, E. C. M. (2015). The mesosphere and metals: Chemistry and changes. *Chemical Reviews. Special Issue: 2015 Chemistry in Climate*, *115*(10), 4497–4541. https://doi.org/10.1021/cr50051m

Qian, L., Solomon, S. C., & Kane, T. J. (2009). Seasonal variation of thermospheric density and composition. *Journal of Geophysical Research*, *114*(A1), A01312. https://doi.org/10.1029/2008JA013643

Smith, A. K., Garcia, R. R., Marsh, D. R., & Richter, J. H. (2011). WACCM simulations of the mean circulation and trace species transport in the winter mesosphere. *Journal of Geophysical Research*, *116*(D20), D20115. https://doi.org/10.1029/2011JD016083

Vadas, S. L. (2013). Compressible f-plane solutions to body forces, heatings, and coolings, and application to the primary and secondary gravity waves generated by a deep convective plume. *Journal of Geophysical Research: Space Physics*, *118*(5), 2377–2397. https://doi.org/10.1002/jgra.50163

Vadas, S. L., & Becker, E. (2018). Numerical modeling of the excitation, propagation, and dissipation of primary and secondary gravity waves during wintertime at McMurdo Station in the Antarctic. *Journal of Geophysical Research: Atmospheres*, *123*(17), 9326–9369. https://doi.org/10.1029/2017JD027974

Vadas, S. L., Zhao, J., Chu, X., & Becker, E. (2018). The excitation of secondary gravity waves from local body forces: Theory and observation. *Journal of Geophysical Research: Atmospheres*, *123*(17), 9296–9325. https://doi.org/10.1029/2017JD027970

Vincent, R. A., & Fritts, D. C. (1987). A climatology of gravity wave motions in the mesopause region at Adelaide, Australia. *Journal of the Atmospheric Sciences*, *44*(4), 748–760. https://doi.org/10.1175/1520-0469(1987)044<0748:ACOGWM>2.0.CO;2

Walterscheid, R. L. (1981). Dynamical cooling induced by dissipating internal gravity waves. *Geophysical Research Letters*, *8*(12), 1235–1238. https://doi.org/10.1029/GL008i012p01235

Walterscheid, R. L., & Hocking, W. K. (1991). Stokes diffusion by atmospheric internal gravity waves. *Journal of the Atmospheric Sciences*, *48*(20), 2213–2230. https://doi.org/10.1175/1520-0469(1991)048<2213:SDBAIG>2.0.CO;2

Walterscheid, R. L., & Schubert, G. (1989). Gravity wave fluxes of O_3 and OH at the nightside mesopause. *Geophysical Research Letters*, *16*(7), 719–722. https://doi.org/10.1029/GL016i007p00719

Weinstock, J. (1976). Nonlinear theory of acoustic-gravity waves, I. Saturation and enhanced diffusion. *Journal of Geophysical Research*, *81*(4), 633–652. https://doi.org/10.1029/ja081i004p00633

Weinstock, J. (1983). Heat flux induced by gravity waves. *Geophysical Research Letters*, *10*(2), 165–167. https://doi.org/10.1029/GL010i002p00165

Weinstock, J. (1990). Saturated and unsaturated spectra of gravity waves and scale-dependent diffusion. *Journal of Atmospheric Science*, *47*(18), 2211–2225. https://doi.org/10.1175/1520-0469(1990)047<2211:sausog>2.0.co;2

Winters, K. B., & D'Asaro, E. A. (1996). Diascalar flux and the rate of fluid mixing. *Journal of Fluid Mechanics*, *317*, 179–193. https://doi.org/10.1017/S0022112096000717

Xu, J., Smith, A. K., & Ma, R. (2003). A numerical study of the effect of gravity wave propagation on minor species distributions in the mesopause region. *Journal of Geophysical Research*, *108*(D3), 4119. https://doi.org/10.1029/2001JD001570

Erratum

The originally published version of this article contained typographical errors. In the PDF version of the article, in Equations 4, 7, 8, 9, 18, 33, 34, B1, B3, B4, C3, C4, and C5 the underbar was missing from vector quantities $\underline{V}$, $\overline{\underline{V}}$, and $\underline{V}'$. In the first sentence of the fourth paragraph of Section 2, "(ρ_C)" should be (ρ'_C)." In the third sentence of the fourth paragraph of Section 2, the underbars were missing from all the vector quantities. In the last sentence of the fifth paragraph of Section 2, "$\left(\nabla \cdot V'\right)$ should be changed to "$\left(\nabla \cdot \underline{V}'\right)$." In the second sentence of the second paragraph of Section 3, "Equation 7–8 into Equation 7–8" should be changed to "Equation 16 into Equation 15." In the first sentence of the third paragraph of Section 3, "Equation 7–8 into Equation 7–8" should be changed to "Equation 18 into Equation 8." In the second sentence of the fourth paragraph of Section 3, "V'" should be changed to "$\underline{V}'$." In the third sentence of the fourth paragraph of Section 3, "Because Equation 7–8 is a linear equation" should be changed to "Because Equation 18 is a linear equation." In the second sentence of the first paragraph of Section 4, "$\left(\nabla \cdot V' = 0\right)$" should be changed to "$\left(\nabla \cdot \underline{V}' = 0\right)$." The right-hand side of Equation 35 should be changed to $-\left(K_H + K_{zz} + K_H^m\right)\overline{\nabla\theta' \cdot \nabla\theta'}$. In the last sentence of the second paragraph of Section 6, "Equations 27–32 and 36" should be changed to "Equations 27, 32, and 36." In the last sentence of Appendix A, "Equation A1–A2" should be changed to "Equation 12." The left-hand side of Equation B6 should be changed to $\overline{w'\theta'_0}$. In the last sentence of Appendix B, "Equation B6–B8" should be changed to "Equation B5." In the last sentence of the second paragraph in Appendix C, "Equation C11–C12" should be changed to "Equation C6." In both online and PDF the term "inject rates" in the last sentence of the third paragraph of section 1 should be "injection rates." The term "at the SOR" in the first sentence of the first paragraph of section 6 should be "at the Starfire Optical Range." In the left-hand side of equation A5, "$\overline{w'\delta'_C}$" should be changed to "$\overline{w'\delta_C}$". In the last sentence of Appendix A the term "$\overline{w'\delta'_C}$" should be changed to "$\overline{w'\delta_C}$." In the right hand side of equation B6, "$\overline{w'\theta'_0}$" should be changed to "$\overline{w'\theta_0}$." The left hand side of equation B6, "$\overline{w'\theta'_0}$" should be changed to "$\overline{w'\theta_0}$." In the PDF version the second sentence in the first paragraph of Appendix A, "ρ_C" should be "ρ'_C". The errors have been corrected, and this may be considered the authoritative version of record.